Chem Soc Rev



REVIEW ARTICLE

View Article Online



Cite this: Chem. Soc. Rev., 2021, **50**, 1251

Methane activation by ZSM-5-supported transition metal centers

Daniyal Kiani, (1) †a Sagar Sourav, (10) †a Yadan Tang, b Jonas Baltrusaitis (10) a and Israel E. Wachs (10) *a

This review focuses on recent fundamental insights about methane dehydroaromatization (MDA) to benzene over ZSM-5-supported transition metal oxide-based catalysts (MO_x/ZSM-5, where M = V, Cr, Mo, W, Re, Fe). Benzene is an important organic intermediate, used for the synthesis of chemicals like ethylbenzene, cumene, cyclohexane, nitrobenzene and alkylbenzene. Current production of benzene is primarily from crude oil processing, but due to the abundant availability of natural gas, there is much recent interest in developing direct processes to convert CH₄ to liquid chemicals. Among the various gas-to-liquid methods, the thermodynamically-limited Methane DehydroAromatization (MDA) to benzene under non-oxidative conditions appears very promising as it circumvents deep oxidation of CH₄ to CO₂ and does not require the use of a co-reactant. The findings from the MDA catalysis literature is critically analyzed with emphasis on in situ and operando spectroscopic characterization to understand the molecular level details regarding the catalytic sites before and during the MDA reaction. Specifically, this review discusses the anchoring sites of the supported MO_x species on the ZSM-5 support, molecular structures of the initial dispersed surface MO_x sites, nature of the active sites during MDA, reaction mechanisms, rate-determining step, kinetics and catalyst activity of the MDA reaction. Finally, suggestions are given regarding future experimental investigations to fill the information gaps currently found in the literature.

Received 7th August 2020 DOI: 10.1039/d0cs01016b

rsc.li/chem-soc-rev

[†] D. K. and S. S. contributed equally.



Daniyal Kiani

Daniyal Kiani received his B.S. in chemistry from Georgetown University, DC, USA. He is currently the John C. Chen Endowed Fellow and a Ph.D. candidate in the Department of Chemical & Biomolecular Engineering at Lehigh University, PA, USA. For his dissertation project, he has been working on synthesizing, characterizing (in situ, operando), testing, and modelling (DFT) tungsten oxide-based catalysts for the oxidative

coupling of methane (OCM) to generate direct structure-function relationships. Besides OCM, he has also studied catalytic ethylene dimerization/oligomerization over heterogenized amminemolecular catalysts, dry methane reformation via DBD-plasma activation, and nutrient recovery via struvite crystallization from wastewater.



Sagar Sourav

Sagar Sourav earned his Bachelor of Technology from National Institute of Technology Rourkela and Master of Technology from Indian Institute of Technology Kanpur, bothin Chemical Engineering. Currently, he is a PhD candidate in the department of Chemical and Biomole-Engineering, Lehigh University, working under the supervision of Professor Israel E. Wachs. He is also the recipient of Graduate Fellowship award from

Idaho National Laboratory. His current research interest includes understanding of molecular structural dynamics of supported W-oxide based catalysts for oxidative coupling of methane and design of Cr-free, Fe-oxide based catalysts for High-Temperature Water-Gas Shift reaction.

^a Department of Chemical and Biomolecular Engineering, Lehigh University, Bethlehem, PA, 18015, USA. E-mail: iew0@lehigh.edu

^b Cummins, Inc. 1900 McKinley Avenue, Columbus, Indiana, 47201, USA

Review Article Chem Soc Rev

1. Introduction

The current abundance of natural gas (NG) across the globe, from recent discoveries of large shale gas deposits in North America and methane hydrates beneath permafrost or in shallow sediments along deep-water continental margins, is projected to persist in the coming years due to improvements in both exploration and extraction technologies. Owing to the large surplus, NG is anticipated to serve as the primary energy resource in the transition period, as the global economies transition off oil-based energy generation to renewable energy-based economies of the future.2 Currently, however, NG is either used as the fuel for power generation and transportation or simply flared to the atmosphere, owing to a deficiency of industrially feasible on-site conversion processes. In the past decades, various attempts have been made to convert methane (CH₄), the primary component (\sim 70-90%) of NG, to value-added products. A schematic summary of the direct CH₄ conversion methods to produce olefins, aromatics and commodity chemicals is presented in Fig. 1. Among these processes, literature reports on the following can be found: methane to methanol and formaldehyde via partial oxidation (POM),2 (ii) methane to ethane and ethylene via oxidative coupling (OCM),³⁻⁶ (iii) methane to benzene via non-oxidative methane dehydro-aromatization (MDA, also known as DHA),⁷⁻⁹ (iv) methane to olefins, aromatics, and hydrogen (MTOAH), 10,11 and methane to halogenated derivates via methane oxyhalogenation. 12-14 Note that although there are various indirect processes to valorize CH₄ like the industrially employed syngas process, they are simply more capital intensive and exhibit a larger carbon footprint than potential direct conversion processes.3,12,14 Given that a significant portion of the total NG is located in stranded locations, building large scale syngas plants remains unfeasible, leading to hundreds of billions of cubic meters of NG being flared from a lack of direct conversion methods. 15 In the past decade, policymakers have moved to reduce NG flaring practices across the globe by introducing regulations and initiatives like the popular Zero Routine Flaring by 2030 initiative, 16 further fueling the research on direct catalytic CH₄ valorization processes.

Metal oxides supported on ZSM-5 constitute an essential class of versatile catalysts that continues to receive both academic and industrial researchers' attention owing to the various reactions they catalyze.^{7,17–29} For example, VO_x/ZSM-5 catalysts have been studied for selective catalytic reduction (SCR) of NO_x with NH₃, ¹⁷ CrO_x/ZSM-5 catalysts are effective for oxidative dehydrogenation (ODH) of ethane to ethylene with CO2, 26 MOOx/ZSM-5 have been investigated for non-oxidative methane dehydroaromatization (MDA) and partial oxidation of methane to formaldehyde, ¹⁹ WO_x/ZSM-5 have been examined for methane oxidation and non-oxidative MDA, 30,31 ReOx/ZSM-5 have been studied for the conversion of ethane to benzene and MDA, ^{24,29} ZnO_r/ZSM-5 catalysts have been found to catalyze the aromatization of alkanes and alcohols,32 etc. This review focuses on a subset of the broader zeolite catalysis literature, i.e., ZSM-5-supported transition metal oxides (MO_x/ZSM-5) where M can be V, Cr, Mo, Re, W or Fe, specifically for MDA to produce benzene. Very recently, ZSM-5 supported group IX (CoO_x/ZSM-5)³³ and group X (NiO_x/ZSM-5)³⁴ catalysts have also been found to be active towards MDA reaction. However, they will not be covered in this review since presently little molecular-level information about these catalysts based on in situ and operando characterization including Raman spectroscopy, X-ray absorption spectroscopy (XAS), etc. is available.

MDA with supported MoO_x/ZSM-5 catalysts was first reported in 1993.8 However, alkanes-to-benzene conversion using zeolite-based catalysts, in general, was actually pioneered in the period of 1974-1989 by a Russian group, which has



Jonas Baltrusaitis

Jonas Baltrusaitis received his Ph.D. from the University of Iowa in 2007. He is currently an associate professor in chemical engineering where he focuses on catalytic natural gas conversion and upgrading. His research approach combines synthesis of catalyst materials and their structure/property determination operating conditions. Additionally, he utilizes density functional theory (DFT) to provide better understanding of

the catalytic material functionality and a rational design approach. He is a recipient of Lehigh University's Libsch Early Career Research Award, Lehigh University's P. C. Rossin Assistant Professorship, and the ACS Sustainable Chemistry and Engineering Lectureship award in 2020.



Israel E. Wachs

Israel E. Wachs studied chemical engineering at City College of the City University of New York and Stanford University. After several years at Exxon, he joined Lehigh University's Department Chemical & Biomolecular Engineering where he is the G. Whitney Snyder endowed professor and director of the Operando Molecular Spectroscopy & Catalysis Laboratory. He has received numerous awards for research on the determination of

electronic and molecular structures of catalytic active sites and their relationship to specific catalytic activity/selectivity (ACS Olah Award in Hydrocarbon or Petroleum Chemistry, Herman Pines Catalysis Award, AIChE Catalysis and Reaction Engineering Practice Award, EPA Clean Air Excellence Award).

Chem Soc Rev Review Article

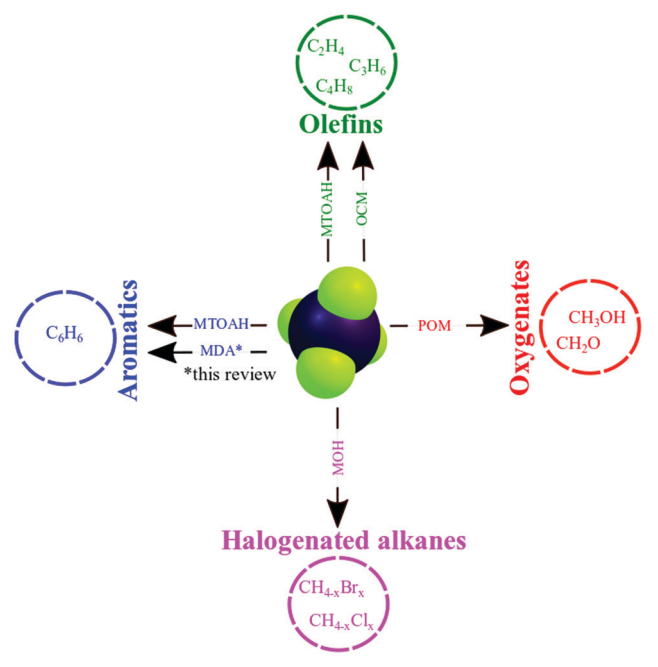


Fig. 1 Direct routes for CH₄ valorization

largely been unrecognized.35-37 Compared to other direct, oxidative processes, the non-oxidative environment for benzene production from methane sparked great interest due to its high product selectivity. This pioneering work, since then, has inspired investigations of other similar catalyst systems composed of group V-VII transition metal oxides supported on zeolite. A few excellent reviews on methane dehydroaromatization (MDA) over zeolite supported transition metal oxide-based catalysts are available in literature 38-41 and the readers are directed to go over them to gain more insights on the following: (i) development of various conventional (Mo-oxide based catalysts) and novel supported catalysts for MDA, including but not limited to the variation of the zeolite support material (e.g. ZSM-5, MCM-22, MCM-49, NU-87, TNU-9 etc.), (ii) the structure and nature of the active sites; (iii) thermodynamics of MDA reaction with associated MDA reaction mechanism and performance of various catalysts; and (iv) catalyst deactivation, coke formation and regeneration methods.

Despite extensive characterization studies reported on supported MO_x/ZSM -5 catalysts, many fundamental details such as MO_x anchoring sites, molecular and electronic structures of MO_x and their responses to different reactive environments remain moot. The lack of consensus about the fundamental details of supported MO_x/ZSM -5 catalysts is strongly related to limited *in situ* studies since most of the characterization measurements were collected under ambient or *ex situ* conditions where the samples are hydrated and not representative of the catalyst structures present under elevated temperatures and reactant gas(es).

The objective of this review is to critically analyze and summarize recent developments in MDA catalysis with emphasis on fundamental *in situ* and *operando* spectroscopy studies in the literature on ZSM-5-supported metal oxide MO_x (M = V, Cr, Mo, W, Re and Fe) catalysts. Specifically, this review discusses

the anchoring sites of MO_x , molecular and electronic structures of the supported MO_x sites, the nature of the active catalytic site(s) before and during MDA, reaction kinetics, rate-determining steps, and reaction mechanism of MDA.

2. Anchoring sites of surface MO_x species on ZSM-5 support

A plethora of studies has focused on elucidating the location of the dispersed MO_r sites in the zeolite matrix in ZSM-5supported catalysts, given the variety of various anchoring sites possible, schematically described in Fig. 2. Generally, (Al-OH⁺-Si) sites with IR band between 3608-3610 cm⁻¹ serve as the anchoring sites internally in the 10 M pores of ZSM-5.42 Outside the pores on the zeolite's surface, the Si-OH (sometimes denoted as Siex-OH in the literature) indicated by IR band at 3745 cm⁻¹, and Al–OH from extra framework Al (sometimes denoted as Alex in the literature) or Al2O3 nanoparticles with IR bands at 3660, 3783 cm⁻¹, respectively, can also serve as the anchoring sites.42 It is generally agreed that the metal oxide sites anchor at either the Brønsted acid sites inside the zeolite channels (-Al-OH⁺-Si-) and/or at the external (-Si_{ex}-OH), with the distribution between internal and external anchoring sites dependent on the synthesis method and Si/Al ratio. 9,31,43 In past studies, the anchoring sites of supported MO_x species (such as WO_x, MoO_x and ReO_x) were determined from the titration of residual zeolite protons, where the MOx species were assumed to have only one type of site. 31,44,45 In contrast, this section on the anchoring sites of supported metal oxides on ZSM-5, emphasized on insights generated via in situ characterization of the catalysts under dehydrated conditions. Studies undertaken in ambient conditions will not be covered since such hydrated catalysts are not relevant to reaction conditions. A detailed discussion of the literature findings is given below, and a summary of anchoring sites for supported MO_x/ZSM-5 catalysts is presented in Table 1.

Supported VO_x/ZSM-5

The anchoring sites in VO_x/ZSM-5 catalysts are affected by the preparation method, as confirmed via in situ (room temperature measurements after high-temperature treatment, without exposing to air) spectroscopic techniques in various reports. 9,46,47 Using IR spectroscopy (spectra collected at room temperature, under vacuum, after dehydration at 773 K), it was shown that the samples prepared by impregnation mainly led to the consumption of external silanol groups in the zeolite. In contrast, samples prepared via solid-state reaction of VCl₃ and H-ZSM-5 primarily resulted in the consumption of framework Brønsted acid sites. Moreover, a monotonic decrease in the framework Brønsted acid sites was observed, via in situ IR spectroscopy, with an increase in the V/Alframework ratio, along with complete consumption of external silanol groups during solid ion exchange by sublimation of VOCl₃ onto ZSM-5. 46 Stoichiometrically, the introduction of each V-atom replaced

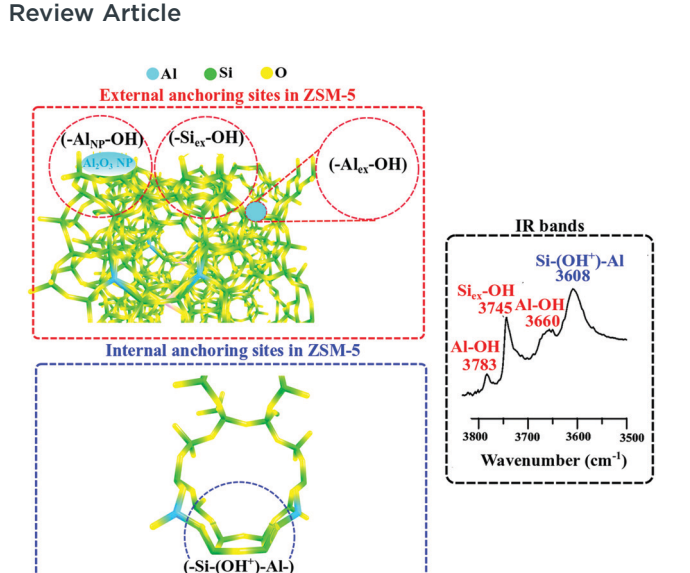


Fig. 2 Types of external and internal anchoring sites and their corresponding IR bands, present in H-ZSM-5 zeolite. Hydrogen atoms are not shown here for clarity.

 ~ 1 proton of the Brønsted acid sites (Al-(OH)⁺-Si) in the zeolite.

Supported CrO_x/ZSM-5

An in situ diffuse reflectance infra-red Fourier transform spectroscopy (DRIFTS)⁴⁸ characterization of supported CrO_x/ ZSM-5 (Si/Al = 15) catalysts, synthesized by solid-state exchange of various chromium salts (Cr-nitrate, Cr-acetate, Cr-chloride, etc.) and ZSM-5, found that the CrO_x species are mainly present at the Brønsted acid sites within the zeolitic pores, with a small amount of CrOx species present at the external silanol sites of the ZSM-5 support. 48 In contrast, a recent in-depth study 49 combining computational, in situ, and operando spectroscopic characterization (IR, Raman, Ultraviolet-Visible Diffuse Reflectance Spectroscopy (UV-vis DRS)) of supported CrO_x/ZSM-5 catalysts with varying Cr-loading and Si/Al ratios found that CrO_x species preferentially anchors at Si-OH sites on the external surface of the zeolite at higher Cr-weight loading (above 0.5 wt%) and when the Al-framework site concentration in ZSM-5 was low (Si/Al = 140). 49

Supported MoO_x/ZSM-5

It is generally accepted in the literature that both framework Brønsted acid sites (Al–(OH)⁺–Si) and external silanol (Si–OH) groups serve as the anchoring sites for MoO_x species on ZSM-5.^{50,51} However, the migration of the MoO_x between various surface hydroxyl anchoring sites is still unresolved. For example, it was reported from *in vacuo in situ* IR measurements that MoO_x is equally distributed at both framework Brønsted acid sites and silanol hydroxyls for low loading cases (<3 wt%) and preferentially anchored at framework Brønsted acid sites for dehydrated catalysts with 6% MoO_x/ZSM -5 (Si/Al = 25).⁵² In another *in situ* IR spectroscopy study, on supported 2% MoO_x/ZSM -5 (Si/Al = 25) catalysts synthesized by impregnation,

it was found that MoO_r migrates from external silanols and extra-framework Al-OH hydroxyls to framework Brønsted acid sites Al-OH⁺-Si at elevated calcination temperatures.⁵³ Preparation from a physical mixture of MoO₃ and ZSM-5, however, indicates the presence of residual framework Brønsted acid sites Al-OH⁺-Si even after calcination at elevated temperatures, reflecting a synthesis-dependent anchoring of MoO_x sites. 44,45 It was also assumed that MoO_r anchored as surface Mo₂O₅ dimers at two adjacent framework Brønsted acid sites, but no direct supporting spectroscopic information was provided about the structure of the MoO_x species and the anchoring sites on ZSM-5.44,45 Moreover, the probability of finding two adjacent Al framework Brønsted acid sites required for anchoring surface dimeric Mo2O5 is very low according to Lowenstein's rule.⁵⁴ Typically, framework Brønsted acid sites in 10 M rings are either isolated or separated by at least two Si atoms as in Al-OH+-Si-O-Si-OH+-Al.55 Therefore, enough paired Al-OH⁺-Si-OH⁺-Al sites will not be present for anchoring at high loadings of MoO_x on ZSM-5 making the anchoring of such dimeric sites very unlikely. More recently, systematic computational and experimental studies on supported MoO_x/ ZSM-5 catalysts have conclusively elucidated the anchoring sites as a function of Mo loading and zeolite Si/Al ratio with in situ IR. 42,56 The IR spectra demonstrated that the MoO_x species preferentially anchor at zeolitic Brønsted acid sites for low Mo oxide loading and anchor to external Si-OH sites for higher Mo loadings, indicating external Si-OH sites can also serve as additional anchoring sites. In addition, Mo deposition can also cause some dealumination of the zeolite framework, and a small fraction of MoOx can also anchor on the extraframework Al-OH sites. 42,56 These findings were also corroborated by a recent in situ IR spectroscopy study.⁵⁷ The MoO_x sites, generated by physical mixing of MoO₃ and H-ZSM-5 followed by calcination, were found to anchor at Brønsted acid sites of the ZSM-5 support. 57 Consequently, the surface MoO_x anchor at multiple surface hydroxyls and not selectively at one kind of surface hydroxyl.

Supported WO_x/ZSM-5

In situ IR study shows that the anchoring sites for WO_x species on ZSM-5 support depends on the preparation method.⁹ For WO_x/ZSM-5 catalyst prepared by the solid-state ion exchange method, the Brønsted acid sites Al-OH+-Si were mainly affected, suggesting anchoring of WO_x species on these sites. The catalysts prepared by the impregnation method, however, were found to be mostly anchored at the external Si-OH surface hydroxyls. In another study,⁵⁸ where the supported WO_x/ZSM-5 catalyst was prepared by incipient-wetness impregnation of (NH₄)₂WO₄ (dried at 393 K for 2 h and calcined at 773 K for 5 h), the effect of WO_x on the Brønsted acidity of ZSM-5 was probed with NH3-temperature programmed desorption (TPD). Only a small change in the desorption temperature and peak intensity for NH3 desorption was noticed, suggesting WOx might be anchored to the Brønsted acid sites of the H-ZSM-5 (Si/Al = 38) support. This indirect characterization method, however, was unable to distinguish between Brønsted acidity

Chem Soc Rev **Review Article**

Table 1 Reported anchoring sites of surface MO_x species in supported MO_x/ZSM-5 catalysts based on IR spectroscopy

		Ref.	
Incipient-wetness impregnation of NH ₄ VO ₃	-Si _{ex} -OH	9	
Solid-state ion exchange	-Al-OH ⁺ -Si-	9	
CrO _x /ZSM-5 Incipient-wetness impregnation of CrO ₃ Solid-state ion exchange Solid-state ion exchange	-Si _{ex} -OH	9	
	$-Al_{ex}$ $-OH^+$ $-Si-$	9	
	Primary: -Al-OH ⁺ -Si- Secondary: -Si _{ex} -OH	48	
Incipient wetness impregnation of (Cr(NO ₃) ₃ ·9H ₂ O	-Si _{ex} OH and -Al-OH ⁺ -Si-	49	
Incipient-wetness impregnation of (NH ₄) ₆ Mo ₇ O ₂₄	-Si _{ex} -OH	9	
Solid state ion exchange	-Al-OH ⁺ -Si-	9	
Thermal spreading of MoO ₃ onto ZSM-5	-Al-OH ⁺ -Si-	57	
Incipient-wetness impregnation of (NH ₄) ₆ Mo ₇ O ₂₄ ·4H ₂ O	High loading: –Si _{ex} –OH low loading: –Al–OH ⁺ –Si–	42	
Solid-state ion exchange	$-Al-OH^+-Si-$	9	
Incipient-wetness impregnation of $(NH_4)_{10}H_2(W_2O_7)_6$	-Si _{ex} -OH	9	
Incipient-wetness impregnation of $(NH_4)_2WO_4$	-Al-OH ⁺ -Si-	58	
Vapor-phase exchange of Re ₂ O ₇	$-Al-OH^+-Si-$	24 and 5	
Incipient wetness impregnation of NH ₄ ReO ₄	Primary: -Al-OH ⁺ -Si-secondary: -Si _{ex} -OH	59	
CVD of FeCla	-Al-OH ⁺ -Si-	65 and 6	
•		9 and 67	
		9	
	Incipient-wetness impregnation of CrO ₃ Solid-state ion exchange Solid-state ion exchange Incipient wetness impregnation of (Cr(NO ₃) ₃ ·9H ₂ O Incipient-wetness impregnation of (NH ₄) ₆ Mo ₇ O ₂₄ Solid state ion exchange Thermal spreading of MoO ₃ onto ZSM-5 Incipient-wetness impregnation of (NH ₄) ₆ Mo ₇ O ₂₄ ·4H ₂ O Solid-state ion exchange Incipient-wetness impregnation of (NH ₄) ₁₀ H ₂ (W ₂ O ₇) ₆ Incipient-wetness impregnation of (NH ₄) ₂ WO ₄ Vapor-phase exchange of Re ₂ O ₇	Incipient-wetness impregnation of CrO_3 $-Si_{ex}$ -OH $-Al_{ex}$ -OH $^+$ -Si-Secondary: $-Si_{ex}$ -OH Incipient wetness impregnation of $(Cr(NO_3)_3 \cdot 9H_2O)$ $-Si_{ex}OH$ and $-Al$ -OH $^+$ -Si-Incipient-wetness impregnation of $(NH_4)_6Mo_7O_{24}$ $-Si_{ex}OH$ $-Al$ -OH $^+$ -Si-Incipient-wetness impregnation of $(NH_4)_6Mo_7O_{24}$ $-Si_{ex}OH$ $-Al$ -OH $^+$ -Si-Incipient-wetness impregnation of $(NH_4)_6Mo_7O_{24} \cdot 4H_2O$ $-Al$ -OH $^+$ -Si-Incipient-wetness impregnation of $(NH_4)_6Mo_7O_{24} \cdot 4H_2O$ $-Al$ -OH $^+$ -Si-Incipient-wetness impregnation of $(NH_4)_1OH_2(W_2O_7)_6$ $-Al$ -OH $^+$ -Si-Incipient-wetness impregnation of $(NH_4)_1OH_2(W_2O_7)_6$ $-Si_{ex}OH$ $-Al$ -OH $^+$ -Si-Incipient-wetness impregnation of $(NH_4)_2WO_4$ $-Al$ -OH $^+$ -Si-Incipient wetness impregnation of $(NH_4)_2WO_4$ $-Al$ -OH $^+$ -Si	

of the ZSM-5 support and new Brønsted acid sites that might have been created by anchoring of the WO_x species (3 wt% WO_x, prepared by incipient-wetness impregnation). A different study proposed that the WO_x species requires two framework Brønsted acid sites on ZSM-5.31 However, this conclusion was solely based on titration of the residual protons of ZSM-5 support and lacked any direct spectroscopic supporting evidence. In conclusion, identification of anchoring sites in WO_r/ZSM-5 catalysts is, thus, pending modern in situ characterization measurements.

Supported ReO_x/ZSM-5

The anchoring sites of dispersed ReO_x for supported ReO_x/ZSM-5 catalysts have received limited attention. In situ IR studies reported that supported ReO_x species preferably anchor at the zeolitic Brønsted acid sites, with a small amount of ReOx species also anchoring at the external silanols. 24,59,60 In situ XAS data in the report corroborated the presence of isolated ReO₄ in ReO_x/ZSM-5, 24 while no direct evidence regarding the proposed dimeric Re₂O_v species⁵⁹ could be found in the literature. Furthermore, it should be noted that dimeric Re₂O_v species are volatile^{61,62} and will not remain on the catalyst surface upon formation, especially at elevated temperatures. 63,64

Supported FeO_x/ZSM-5

The surface FeO_x species of the supported FeO_x/ZSM-5 catalysts were found to be anchored within the zeolitic pores of ZSM-5 and are dependent on the preparation method. Chemical vapor deposition (CVD) of FeCl₃, followed by washing and calcination, results in dispersed FeO_x/ZSM-5 catalysts at high Fe loading. 65,66 The in situ IR results of these catalysts revealed that the FeO_r species anchored at the framework Brønsted acid sites. Other studies employing solid-state ion exchange and in situ IR revealed the consumption of framework Brønsted acid sites upon

anchoring of FeO_x. 9,67 In contrast, in situ IR data of the supported FeOx/ZSM-5 catalysts, prepared by the impregnation method, evidenced the preferential anchoring of FeO_r species at external Si-OH sites.9

3. Nature of surface MO_x sites in supported MO_v/ZSM-5 catalysts before MDA

Various literature reports for ZSM-5 supported MO_r catalysts discuss the nature of metal oxide sites within the zeolitic pores. Typically, in situ and operando spectroscopic techniques such as Raman, UV-vis DRS, XAS, etc. have been used to directly probe the structure of the dehydrated and oxidized MO_r sites before MDA. Earlier non-spectroscopic characterization studies employing the indirect method of titration of surface hydroxyls, however, have also been applied to propose the structure of the MO_r sites on ZSM-5. A case-by-case discussion of the nature of surface MO_x sites before MDA in group V-VII metal oxides/ ZSM-5 catalysts is given in the following subsections. The reader should keep in mind that the nature of sites in supported heterogenous catalysts has historically remained controversial in the broader catalysis field because of different approaches employed in trying to assign supported MOx structures. For example, the question of isolated versus dimeric/oligomeric active sites has been heavily debated with regards to CrOx/SiO2type Phillips catalysts. Simple titration study of Si-OH groups by CrO_x suggested the co-existence of both isolated CrO₄ and dimeric Cr₂O₇ species on SiO₂.⁶⁸ More recent characterization studies employing direct advanced in situ spectroscopic characterization, however, conclude that only isolated surface CrO_x sites are present on the SiO₂ support. 69,70 Likewise, no consensus exists regarding the nuclearity of active Cu sites in zeolite supported Cu_xO_y

catalysts used for selective catalytic reduction of NO_x and methane-to-methanol reactions. The selective critically analyzed the state-of-the art literature reports on ZSM-5 supported MDA catalysts and provided our proposals for the structures of the surface MO_x sites on ZSM-5 based on the most advanced supporting data available. We, however, tried to analyze key literature from all sides of the debate to provide the reader with a nuanced understanding of the catalytic active sites in these MDA catalysts. The large variety of anchoring sites on the ZSM-5 support suggests that multiple surface MO_x sites are probably formed for each metal oxide on

Supported VO_x/ZSM-5

ZSM-5.

Review Article

Several molecular structures for dehydrated supported VO_r species on ZSM-5 have been proposed in the literature. Early electron paramagnetic resonance/electron spin resonance (EPR/ESR) measurements evidenced EPR-active V⁴⁺ oxides present on the zeolite. It was hypothesized that isolated VO²⁺ were present on the cationic sites of zeolites via ESR conducted after various treatments like heat treatment (720 K, 6 h, N₂), adsorption of water, or adsorption of ammonia. 74,75 A different study 47 proposed the presence of VO2+ species on both Brønsted acid sites and external silanols. Note, however, that EPR spectroscopy only detects paramagnetic V⁴⁺ species that may be present in trace quantities and not V^{5+}/V^{3+} species that are EPR silent. Moreover, interpreting EPR signals in supported catalysts to conclude isolated vs. dimeric/oligomeric VO_x sites is challenging, given that even the EPR of V₂O₅ single crystals showed significant deviation from expected EPR patterns and exhibited electron sharing between inequivalent V-V neighbors.⁷⁶

In a relatively-recent in situ characterization study, the presence of isolated dioxo $VO_2^{\ +}$ and dimeric $V_2O_4^{\ 2+}$ species located on cationic sites of zeolites for supported VO_x/ZSM-5 (Si/Al ~ 13.4) were proposed based on in situ FT-IR, in situ Raman and EXAFS. 46 The Raman bands in the 1065-1076 cm⁻¹ range were assigned to the terminal V-oxo (V=O) vibration, based on the DFT calculations in the same study. 46 However, experimental Raman of supported VO_r catalysts elsewhere in the literature evidences V=O vibrations at lower wavenumbers.⁷⁷ The terminal V=O bond for mono-oxo O=VO_r sites exhibits only a single Raman band in the 1015-1040 cm⁻¹ range, which is much lower than 1065-1076 cm⁻¹ scale.^{78,79} The V=O bonds in dioxo O=V-O-V=O are expected to be longer than the V=O bond in mono-oxo O=VOx sites and would give rise to V=O vibrations at much lower wavenumbers than 1015-1040 cm⁻¹.80 Additionally, the dioxo O=V-O-V=O structure would give rise to both v_s and v_{as} V=O (a doublet) as well as V-O-V vibrations, which were not observed. The high wavenumber band at 1065-1076 cm⁻¹ reported in ref. 46 might either correspond to Si-O-Si vibration or be blue-shifted due to Raman spectrometer not being calibrated. The proposed dimeric surface V₂O₄²⁺ species, if present, cannot be present in significant abundance since the in situ extended X-ray absorption fine structure (EXAFS) spectra⁴⁶ does not exhibit a V-V peak in the second coordination sphere (i.e., V-O-V) at \sim 3 nm. 81 The X-ray absorption near-edge structure (XANES) part of the spectrum exhibits a clear pre-edge, which is expected for isolated, non-centrosymmetric sites like the mono-oxo O=VO3 sites. As bridged V–O–V bonds form as in dimeric $V_2O_4^{\ 2+}$ sites, the symmetry of the sites should have changed that would lead to a decreased pre-edge intensity. Such a decrease in the pre-edge feature, however, was not observed suggesting that the presence of dimeric surface V_2O_x sites in VO_x/ZSM -5 catalysts is not supported by the XANES spectra.

The in situ UV-vis spectra of dehydrated 3% VO_x/ZSM-5 (Si/Al = 15), prepared by incipient-wetness impregnation, exhibited a strong Ligand-to-Metal Charge Transfer (LMCT) band characteristic of V5+ species82 and a high edge energy value $(E_{\rm g} \sim 3.5 \text{ eV})$ in the region of isolated surface $V^{5+}O_{\rm x}$ sites. Oligomeric $(VO_x)_n$ sites give rise to E_g values of ~ 2.8 –3.2 eV and bulk V_2O_5 exhibits an even lower $E_g \sim 2.3$ eV. 83,84 The corresponding in situ Raman spectrum exhibits only a single, sharp Raman band at ~ 1038 cm⁻¹ that is characteristic of a monooxo V=O stretching vibration,82 which matches the VO₄ (O₃V=O) coordination of dehydrated surface species on other oxide supports. 79,83,85,86 No supporting evidence was found for isolated, dioxo $OV^{5+}(=O)_2$, which would give rise to two bands $(v_s \text{ and } v_{as})$ at lower wavenumber (~1000 cm⁻¹), or dimeric V₂O_x, which would exhibit bridging V-O-V Raman vibrations \sim 250 cm⁻¹ and V-V features in the second coordination of EXAFS, were found. Therefore, it is expected that surface VO_r sites are present within the zeolitic pores of the ZSM-5supported catalysts as isolated, mono-oxo (O₃V⁵⁺=O) surface species, as shown in other supported VO_x catalysts.^{79,83,85,86} A schematic of the molecular structure of the major dehydrated VO_x site on the ZSM-5 support based on in situ spectroscopic evidence for supported VO_x/ZSM-5 is shown in Fig. 3a.

Supported CrO_x/ZSM-5

Early characterization studies employing in situ IR, EPR and Mössbauer spectroscopy under vacuum conditions proposed the presence of both Cr5+ and Cr6+ cations for the supported CrO_x/ZSM-5 catalysts.⁸⁷ It is worth noting, however, that Cr⁶⁺ can readily reduce to Cr5+ under vacuum and may give rise to Cr⁵⁺ signals (e.g., EPR) that are artificially induced by the experimental conditions. Employing in situ XAS (sample sealed in polyethene films under inert atmosphere after treatment with air and taken to the beamline, XAS at 295 K),88 the supported CrO_r/ZSM-5 catalysts prepared *via* wet-impregnation of Cr–nitrate solution into ZSM-5 were investigated. The presence of Cr-O-Cr coordination indicated the presence of Cr2O3 nanoparticles (NPs) for Si/Al ratios of 29-940. In comparison, only isolated surface CrO_x⁶⁺ sites were evidenced for higher Si/Al ratios (>940). Based on the intense pre-edge feature in the XANES portion of the XAS spectrum, the possibility of di-grafted, dioxo O₂Cr(=O)₂ structures present on the ZSM-5 support was proposed for Si/Al ratios of 29-1900. In the same study, complementary EXAFS of the catalysts with Si/Al ~ 29 –1900 corroborated the presence of significant Cr=O bond character in the first coordination shell, but also evidenced weak Cr-O-Cr coordination as in Cr₂O₃ NPs in the second and third coordination shells.⁸⁸ A simplistic schematic, for illustration purpose, of tri-oxo CrO_x

Chem Soc Rev **Review Article**

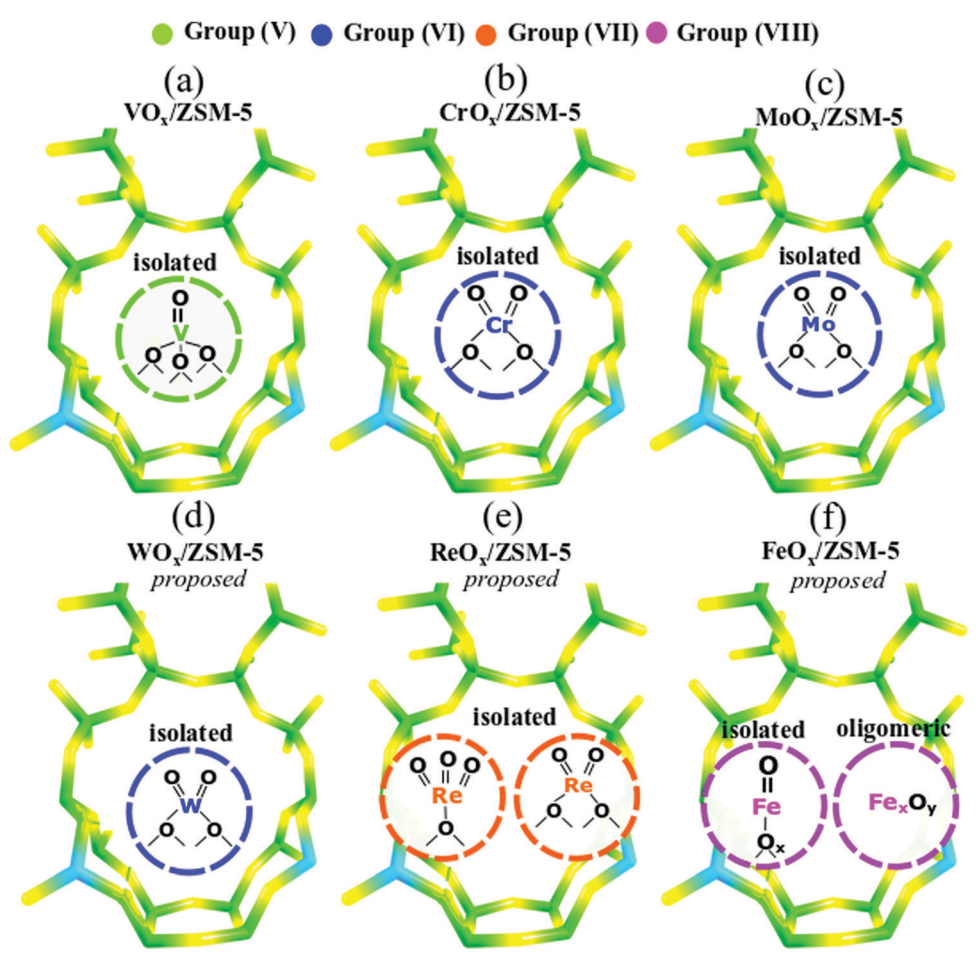


Fig. 3 Schematic summary of molecular structures of the major dehydrated MO_x sites on the ZSM-5 support, based on in situ spectroscopic (Raman, UV-Vis, X-ray absorption) and DFT investigations. These structures represent surface MO_x anchored within the zeolitic pores of MO_x/ZSM-5 catalysts under dehydrated conditions, before MDA reaction, where MO_x is (a) VO_x, (b) CrO_x, (c) MoO_x, (d) WO_x, (e) ReO_x, and (f) FeO_x. Hydrogen atoms are not shown for clarity. Further details and structures of minor species can be found within respective references of subsections under Section 3.

structure has also been proposed in the literature, where the bridging Cr-O-support bond shares an electron with one of the three terminal Cr=O bonds.89 This report warrants some additional discussion since an isolated trioxo Cr(=O)₃ structure would be expected to give rise to four Raman vibrations located at $\sim 908 \ (v_s)$, 933 (v_{as}) , 947 (v_{as}) , and 955 (v_{as}) cm⁻¹ that have been reported for the gas phase tri-oxo CsBrCr(=O)₃ reference compound. 90 Without confirmation from in situ Raman spectroscopy, the surface tri-oxo (O=)3CrO structure cannot be validated and seems highly improbable. The number of Cr=O oxo bonds, however, can be confirmed with Raman spectroscopy during isotopic ¹⁸O₂-¹⁶O₂ exchange since a trioxo (Cr=O)₃ functionality will give rise to band splitting to 4 bands from the isotopic permutations(($=^{16}O$)₃, ($=^{16}O$)₂($=^{18}O$), ($=^{16}O$)($=^{18}O$)₂ and (=18O)3).91 Recently, dehydrated supported CrOx/ZSM-5 catalysts prepared by solid-state reaction (Si/Al = 15, Cr/Al = 0.5, 1 and 1.5) and were characterized with Raman and UV-Vis DR spectroscopy. 48 The Raman band at $\sim 375~\text{cm}^{-1}$ was assigned to oligomeric CrO₂. However, elsewhere in the literature, a similar band is actually assigned to the ZSM-5 support. 92,93

In a more recent in-depth study, the dehydrated supported CrO_x/ZSM-5 catalysts were thoroughly characterized via in situ UV-Vis DR, IR and Raman spectroscopy. 49 For 1 wt% CrO_x/ZSM-5 (Si/Al = 15, 25 and 40) catalyst samples, under O2 flow at 383 K, Raman bands at 964 and 1033 cm⁻¹ were observed, which were assigned to the di-oxo $O_2Cr(=O)_2$ and mono-oxo $O_4Cr(=O)$ structures within the zeolitic pores, anchored on to Brønsted acid sites. For lower concentration of Al (Si/Al = 140), new bands at 984 and 1017 cm⁻¹ were present, which correspond to dioxo O₂Cr(=O)₂ and mono-oxo O₄Cr(=O) structures on Si-sites, respectively, on the external surface of ZSM-5. This observation suggests that lower Al concentration force CrOx to become anchored on the Si sites of the external surface. Further, it should be noted that these spectra were different from the spectra obtained under the same O₂ flow but at a higher temperature of 773 K. At 773 K, for all Si/Al ratios (25, 40 and 140), the catalysts exhibit Raman vibrations at 984 and 1017 cm⁻¹, indicating that exposure to gas-phase O2 at elevated temperatures forces the Cr oxide species within the zeolite pores to migrate to the external surface of the zeolite.49 Migration was only observed when Cr loading was higher than 0.5 wt% since no shift in Raman bands

Review Article Chem Soc Rev

was noticed at lower Cr loading.⁴⁹ A schematic of the molecular structure of the major dehydrated CrO_x sites based on *in situ* spectroscopic (Raman, UV-Vis, X-ray absorption) and DFT for supported $CrO_x/ZSM-5$ is shown in Fig. 3b.

Supported MoO_x/ZSM-5

Multiple MoO_x structures have been proposed for the supported MoO_x/ZSM-5 catalysts. From in situ XAS characterization, ⁴⁵ catalysts prepared by thermal spreading of MoO₃ onto a ZSM-5 (Si/Al = 19) support, bridging Mo-O-Mo bonds in the second coordination shell (Mo-O-Mo) were not observed. It can be argued that dimeric (Mo₂O₅)²⁺ sites were present, and that the absence of a detectable Mo-O-Mo feature was related to destructive interference of the EXAFS signals from Mo and Al neighbors. However, Al is a much lighter element than Mo and, thus, the weaker EXAFS scattering from the Al sites cannot destructively interfere with the much stronger EXAFS scattering from the Mo sites. In the same study, the in situ visible Raman spectra exhibited bands at 970 and 1045 cm⁻¹, which were tentatively assigned to dimeric and isolated MoO_x sites, respectively. Dimeric Mo₂O₅ sites were proposed in another study, where in situ Raman bands at 868 and 962 cm⁻¹ were assigned to the Mo-O-Mo stretching mode of dimers and the terminal M=O stretch in isolated mono-oxo O₄Mo=O sites, respectively.⁹⁴ In contrast, however, the vibration at 868 cm⁻¹ is characteristic of bridging Mo-O-Al/Si vibrations and the vibration at 962 cm⁻¹ is related to terminal Mo=O bonds (most likely dioxo MoO4 sites). 95-97 The oxidation state of the surface MoO_x sites, which some authors tried to characterize with EPR, was not resolved because concrete evidence for the proposed oxidation states could not be obtained. 50 A more recent in situ/operando XAS spectroscopic study found that the dehydrated MoO_x/ZSM-5 catalyst exhibits a strong pre-edge feature with a featureless post-edge regime, which is similar to the Na2MoO4 reference compound consisting of isolated MoO₄ sites. 98 Consequently, it was proposed that the dehydrated MoOx/ZSM-5 catalyst predominantly contains monomeric [MoO₄]²⁻ species and that a minor amount of dimeric Mo-oxo species may also be present without any supporting evidence. In another in situ/operando XAS study of MoO_x/ZSM-5 catalysts, it was reported that at low Mo loading (<2 wt% Mo), only the dispersed Mo-complexes are present within the zeolitic pores, whereas at high Mo loading (5 wt% Mo) large Mo clusters are also present on the external surface of the zeolite support.99

Rigorous characterization studies integrating *in situ* Raman, UV-vis and DFT calculations have provided a more firm picture of the nature of the dehydrated surface MoO_x sites on ZSM-5. A2,56 The isolated nature of the dehydrated surface MoO_x sites on ZSM-5 was demonstrated with *in situ* UV-vis studies that exhibit a high E_g value of ~ 4.9 eV, which is significantly higher than the E_g value expected for dimeric MoO_2O_x (~ 4.0 –4.2 eV) and oligomeric MoO_x (~ 3.5 eV) clusters, and reflects the exclusive presence of isolated surface MoO_x sites. A2,56 The corresponding *in situ* Raman spectra of the dehydrated supported $\text{MoO}_x/\text{ZSM-5}$ catalysts revealed that five distinct surface MoO_x species were present on the ZSM-5 support with the relative population of each surface

 MoO_x structure dependent on both the MoO_x loading and the Si/Al ratio: (i) isolated, di-oxo (OH)O₂Mo(O=)₂ on single Al site inside the 10 M ring, (ii) isolated di-oxo O2Mo(O=)2 on two Al sites within the 10 M ring (iii) isolated di-oxo $O_2Mo(O=)_2$ on external silanols, (iv) isolated, mono-oxo MoO5 species on Al2O3 nanoparticles/clusters on the external surface, (v) isolated, monooxo MoO5 at external defect sites (Siex and Alex). The resulting molecular structures are summarized in Fig. 4. The molecular structural assignments were assisted by detailed DFT calculations (see ref. 42 and 56 for the details). Additionally, crystalline MoO₃ NPs can form at high Mo loadings when all the anchoring sites on ZSM-5 are completely titrated. These in situ spectroscopic findings clearly demonstrate the co-existence of multiple types of "isolated" surface MoO_x sites on the ZSM-5 support and rule out possibility of dimeric Mo_2O_x species. A schematic of the molecular structure of the major dehydrated VO_x site on the ZSM-5 support based on in situ spectroscopic (Raman, UV-Vis, X-ray absorption) and computational insights for supported MoOx/ ZSM-5 is shown in Fig. 3c.

Supported WO_x/ZSM-5

There is a general agreement in the literature regarding the nature of the dispersed WO_x sites present in dehydrated supported WO_x/ZSM-5 catalysts. ^{30,31} UV-vis DRS analysis has shown that the surface WO_x sites are isolated owing to the very high $E_{\rm g}$ value ~ 5.8 eV (LMCT ~ 210 nm). ^{30,31} Tungsten oxide UV-Vis $E_{\rm g}$ values > 5.0 eV correspond to isolated WO_x sites since the $E_{\rm g}$ value for dimeric W₂O_x (~ 4.0 eV) and oligomeric WO_x (~ 3.5 eV) are significantly lower. This conclusion is further supported by *in situ* EXAFS measurements that did not exhibit a second coordination shell comprising W–O–W

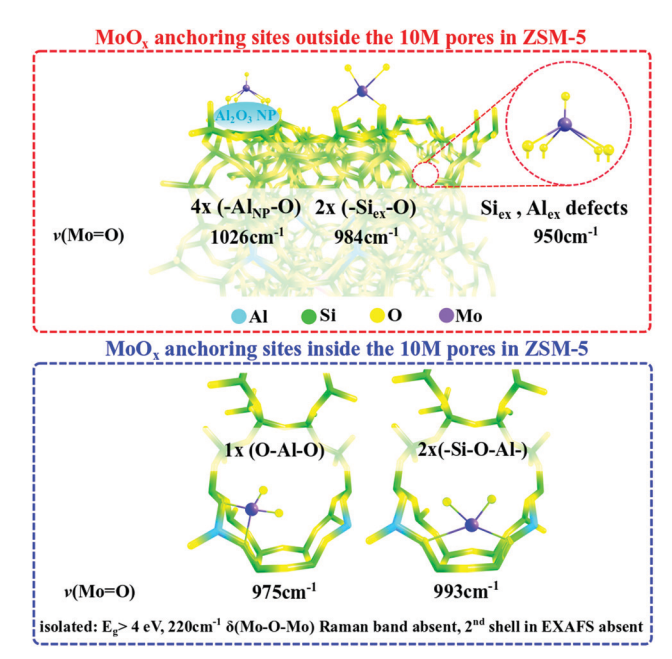


Fig. 4 Unique isolated surface MoO_x sites present in $MoO_x/ZSM-5$ catalysts. The motivation for the schematic has been drawn from the *in situ* spectroscopic and DFT studies reported in ref. 42 and 56.

linkages. 82,100 The *in situ* Raman spectrum of the dehydrated supported WO_x/ZSM-5 catalyst exhibited two Raman bands at \sim 990 and 1020 cm⁻¹ that have been assigned to isolated dioxo O₂W(O=)₂ and mono-oxo O₄W=O species on ZSM-5, 82 respectively, that match WO₄ and WO₅ vibrations of isolated WO_x species on other oxide supports. $^{101-104}$ A schematic of the molecular structure of the most likely dehydrated WO_x site on the ZSM-5 support based on *in situ* spectroscopic (Raman, UV-Vis, X-ray absorption) for supported WO_x/ZSM-5 is shown in Fig. 3d.

Supported ReO_r/ZSM-5

Chem Soc Rev

Based on *in situ* Raman and XAS measurements, it was proposed that supported ReO_x species on ZSM-5 were present as isolated trioxo $\text{ORe}(=-0)_3$ species anchored to one site associated with framework alumina (*e.g.*, Si-O*-Al-O*-Si).^{24,59} The absence of bridging Re-O-Re vibrations for dimeric Re_2O_x , which are expected at \sim 456 (ν_s) and \sim 185 (δ) cm⁻¹ in the Raman spectra, and the absence of Re-O-Re in the second coordination sphere in the EXAFS spectra demonstrate that the surface ReO_x sites are indeed isolated on the ZSM-5 support.

More recent in situ UV-Vis and Raman characterization studies have provided additional insights about the dehydrated surface ReOx sites present in the supported 3% ReOx/ZSM-5 (Si/Al-15) catalyst. 82 The in situ UV-vis spectrum exhibit an E_{g} value of ~ 5.0 eV that is significantly higher than the E_g value of oligomeric $(ReO_x)_n$ structures at 2.8-3.0 eV and confirms the isolated nature of the surface ReO_x sites on ZSM-5.84 The corresponding in situ Raman spectra of the dehydrated ReO_x/ ZSM-5 catalyst possessed two vibrations at 975 and 1010 cm⁻¹ that were assigned to $v_{as}(Re=0)$ and $v_{s}(Re=0)$ vibrations, respectively, of a structure containing multiple Re=O oxo bonds. Additional studies involving isotopic ¹⁸O-¹⁶O exchange and DFT calculations are needed to determine the number of Re=O oxo bonds for the supported ReO_x/ZSM-5 catalysts. 63,64,78 A schematic of the molecular structure of the most likely dehydrated ReO_r sites on the ZSM-5 support based on in situ spectroscopic (Raman, UV-Vis, X-ray absorption) for supported ReO_x/ZSM-5 are depicted in Fig. 3e.

Supported FeO_x/ZSM-5

Preliminary studies on catalysts prepared *via* CVD or solid-state ion exchange, to achieve a high Fe/Al exchange ratio, evidenced various FeO_x sites (isolated (O–Fe–(OH)₂), isolated (O–Fe—O) in distorted tetrahedral coordination, oxygen-bridged dimeric Fe₂O₃(OH)₂, oligomeric FeO_x clusters, and small Fe₂O₃ nanoparticles). A recent *in situ* XAS study, where the absorption data were fitted to crystalline reference compounds, that the FeO_x sites prior to any treatment were present as a mixture of crystalline hematite (Fe³⁺, α -Fe₂O₃) and magnetite (Fe²⁺, Fe³⁺), Fe₃O₄) phases. Upon heating in a He environment to high temperature, the iron oxide structure was reduced to wüstite (Fe²⁺, FeO). This study, however, could not ascertain if dispersed phases of surface FeO_x sites or clusters were also present in the catalyst since XAS is a bulk characterization technique that averages the signal over all types of FeO_x in the

catalyst. Further structural insights are needed with application of molecular spectroscopy that can distinguish between the different types of FeO_x that may be present in the ZSM-5 support (*e.g.*, Raman spectroscopy). A schematic of the molecular structures of the most likely dehydrated FeO_x sites on the ZSM-5 support based on *in situ* spectroscopic (X-ray absorption) for supported $FeO_x/ZSM-5$ are shown in Fig. 3f.

4. Nature of surface MO_x sites in supported $MO_x/ZSM-5$ catalysts during MDA

Only a few *in situ/operando* spectroscopic characterization studies have been reported on the state of the surface MO_x sites in supported $MO_x/ZSM-5$ catalysts during MDA. This is a consequence of the few characterization techniques that can operate under the extreme MDA reaction conditions of 973–1073 K. At such high temperatures, only XAS, XRD and Raman spectroscopy can provide detailed structural information. Other characterization techniques, however, can be applied at much lower temperatures either before or after reaction.

Supported $VO_x/ZSM-5$

Only a limited number of studies have reported on the nature of the VO_x site in supported VO_x/ZSM -5 catalysts during MDA. *In situ* X-ray photoelectron spectroscopy (XPS) surface analysis⁷ of supported VO_x/ZSM -5, under vacuum conditions before and after reaction with methane at 1023 K for 3–4 hours (without exposing the samples to air after treatment), found the presence of reduced V^{3+} cations on the spent supported VO_x/ZSM -5 catalysts. The local geometry and coordination number of these cations, however, cannot be provided by XPS.

Supported $CrO_x/ZSM-5$

Little has been reported on the structure of the activated CrO_x/ZSM-5 catalysts during MDA. An in situ XPS study (samples were treated under the reaction environment, followed by XPS measurements under ultra-high vacuum, without exposing to atmosphere) with a supported 2% CrO_x/ZSM-5 (Si/Al = 25) catalyst showed that the initial Cr6+ oxide sites became partially reduced under reaction with methane and converted to Cr³⁺ oxide sites that remain catalytically active during methane dehydroaromatization at 1023 K.7 A recent operando Raman spectroscopy study during MDA along with computational insights, 49 found that the Raman band at 1033 cm⁻¹ from Cr⁶⁺ mono-oxo species (O_xCr⁶⁺=O) anchored at framework [AlO₄] sites disappeared, suggesting reduction, with appearance of a new Raman band at 1062 cm⁻¹ from organic deposits. The exact nature of the surface Cr sites on ZSM-5 under reaction conditions $(CrC_x \nu s. CrOC_x)$ has still not been elucidated, but the initial Cr⁶⁺ sites reduce to Cr³⁺.

Supported MoO_x/ZSM-5

Multiple in situ and operando 42,56 spectroscopic studies have focused on determining the nature of the active surface Mo

sites during the MDA reaction. 57,98 It is worth noting that since most of the operando spectroscopy studies used XAS to characterize the catalyst, the presence of crystalline MoO₃ NPs cannot be ruled out which complicates the XAS analysis. Additionally, MoO₃ NPs are too large to fit into the pores of ZSM-5 and can easily be converted to large MoC NPs, blocking the pores.⁵⁶ Unless Raman spectroscopy was employed to characterize the initial state of the MoO_r in ZSM-5, the presence of crystalline MoO₃ NPs in the starting material would not be known. Operando XAS studies revealed that during the MDA reaction, the surface MoO_x sites on the ZSM-5 support: (1) partially carburized to intermediate MoO_xC_v oxycarbide clusters, (2) subsequently carburized to MoC_x clusters at longer reaction times, and (3) finally detached from the zeolitic pore to aggregate into Mo_{1.6}C₃ clusters, which was coincident with the maximum benzene production. 107 The Mo_{1.6}C₃ clusters, predominantly on the outer zeolite surface, were then observed to grow further, which appears to be the primary cause of catalyst deactivation. Note that catalyst deactivation from hydrocarbon deposition was recently shown to be reaction parameter-dependent, with higher methane pressures stabilizing the supported Mo/ZSM-5 catalyst. 107 Moreover, MoCx agglomeration was shown to be reversible via operando Raman spectroscopy, with the initially isolated surface MoOx sites essentially completely restored by treatment with gas-phase oxygen post MDA reaction that fully restored the catalytic performance of the supported Mo/ZSM-5 catalysts. 42,56 Both experimental findings and computational calculations confirm the presence of reduced Mo species such as MoO_xC_y and MoC_x, which serve as the active sites during the MDA reaction. 108-112 A recent detailed study employing ¹³C-NMR with isotopically-labelled ¹³CH₄ showed that after activation of 2% MoOx/ZSM-5 and subsequent switching to ¹²CH₄ (with an Ar purge in between) produced a significant amount of ¹³C containing benzene molecules. More than 70% of the benzene molecules formed after the first ¹²CH₄ pulse contained at least one 13C atom, indicating the dynamic and active roles of MoO_xC_y, MO_xC_y and confined carbonaceous species during MDA. 110

Supported WO_x/ZSM-5

Review Article

In situ XAS31 and ex situ high resolution transmission electron microscopy (HR-TEM)¹¹³ studies found poorly-ordered WC_v ($\sim 0.6-1$ nm) present inside the zeolitic pores for WO_x/ZSM-5 catalysts during MDA. An in situ XPS study examined the oxidation state of WOx species on the ZSM-5 support after exposing the catalyst to MDA reaction environment for different amounts of time.7 After 2 h of reaction, slight decreases in the binding energy of W $4f_{7/2}$ and W $4f_{5/2}$ were observed that are consistent with the formation of W5+ oxides. Further exposure to MDA reaction environment (~13 h) showed an additional shoulder \sim 33.5 eV, corresponding to W⁴⁺ site. Interestingly, this study did not evidence the formation of WCx via in situ XPS investigation. Further information on the nature of active surface WO_x sites during MDA is not available, and additional in situ characterization studies using IR, Raman, XAS, and UV-vis DRS are needed as a function of the synthesis method to bridge this information gap.

Supported ReOx/ZSM-5

The active component of supported $\text{ReO}_x/\text{ZSM-5}$ for MDA has attracted little attention in the literature. An *in situ* XAS study²⁴ observed that surface ReO_x species converted to metallic Re clusters ~ 8.2 Å in size, at the initial stage of benzene formation. Given that ~ 8.2 Å is comparable to the pore size of the ZSM-5 support, it is not clear from this study if the reported Re^0 clusters were observed outside or inside the pores. The facile reduction of Re^{7+}O_x to Re^0 in reducing environments is well known.⁶²

Supported FeO_x/ZSM-5

FeO_x/ZSM-5 catalysts were also studied via operando XAS. 106 It was found that benzene only formed after a particular XANES feature was observed. 106 Although the XANES spectrum was similar to that of the reduced form of iron, some unique features, however, did not match any of the measured reference compounds (Fe₃C, Fe₂C₅, or Fe foil). Therefore, the unique XANES feature was tentatively assigned to a reduced/metallic iron phase that can include variable amounts of oxycarbidic carbon (e.g., FeO_xC_v) that was also corroborated with the resemblance of the FT-EXAFS spectrum taken at the end of the MDA reaction with the spectrum of Fe₅C₂ and Fe₃C standards (similar position of the Fe-C and Fe-Fe scattering paths). 106 Facile reduction of iron oxide to metallic Fe⁰ in reducing environments is well established. 114-116 In contrast, only a slightly reduced form of iron oxide (Fe₃O₄) was reported from in situ XPS and EPR studies (catalyst conditioned under MDA reaction at 973 K, spectra collected at room temperature) and formation of carbidic/oxy-carbidic Fe-clusters were not detected. 7,117 In the above studies, the presence of Fe₃O₄ phase in the MDA reaction mixture treated catalyst was confirmed by matching the XPS and EPR spectra of the treated catalysts with the signals of Fe₃O₄ bulk phase in the literature.

5. Activity and structure–function relationships of $MO_x/ZSM-5$ catalysts towards MDA

Comparison of MDA performance of MO_x/ZSM-5 catalysts

For a detailed comparison of steady-state catalytic MDA performance of various transition metal-oxide-based ZSM-5-supported catalysts, the readers are directed to an existing review paper in the MDA literature. Although, in the mentioned article, the catalysts' performance have been compared under different reaction environment, one can clearly see that the MDA activity of $MoO_x/ZSM-5$ catalyst towards benzene production is much higher relative to most other $MO_x/ZSM-5$ catalysts. In the current review, we have tried to critically analyze MDA catalysis literature to generate insights based on reports employing similar reaction conditions or reports where all pertinent experimental information is explicitly reported for us to normalize their data. We compared the benzene production rate per metal atom (turnover frequency (TOF), s^{-1}) for the

Chem Soc Rev

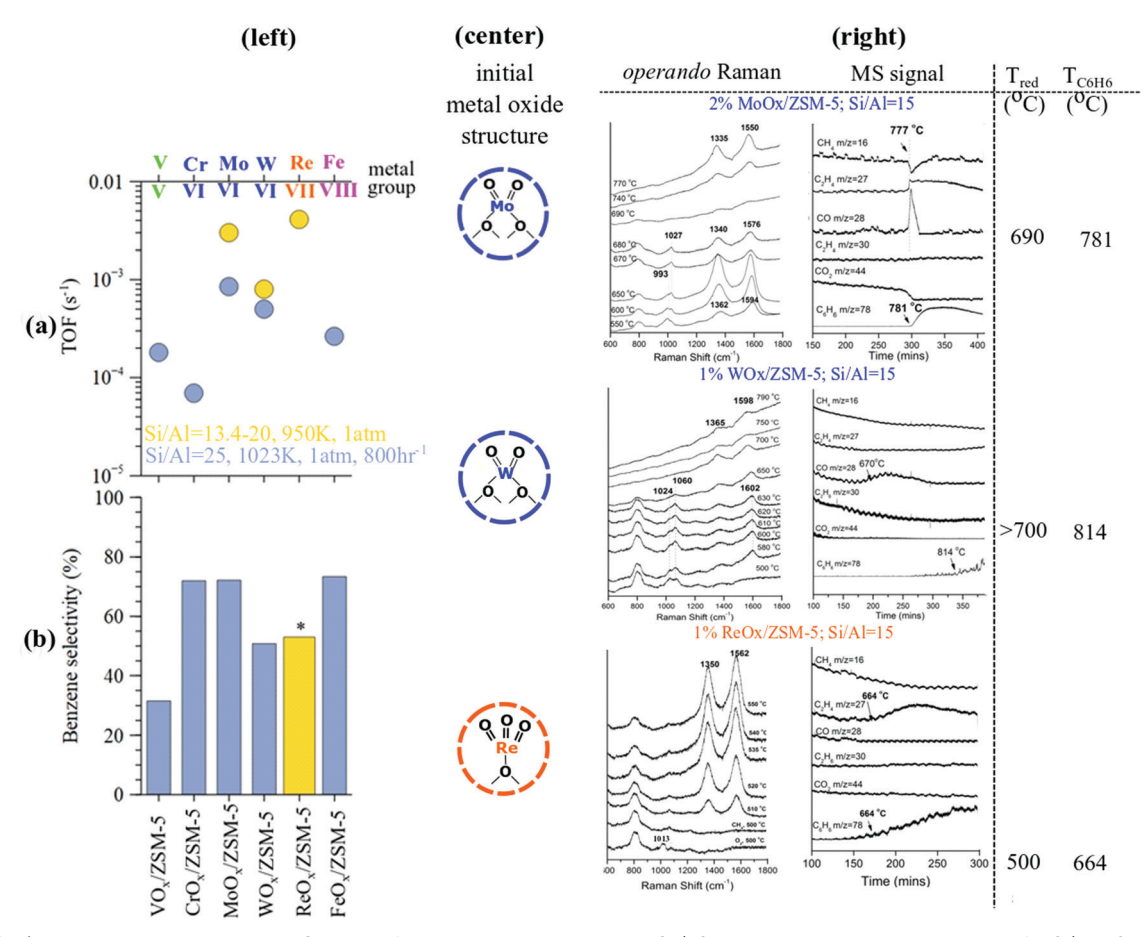


Fig. 5 (Left-a) shows benzene production TOF values for group V-VIII supported MO_x/ZSM-5 catalysts. Experimental details for Si/Al = 25 can be found in ref. 9 and Si/Al = 13.4-20 in ref. 24. For Si/Al = 25, the highest reported CH₄ consumption TOF was divided by the stoichiometric factor of six to approximate the benzene production TOF. Lastly, for Si/Al = 13.4, the CH₄ GHSV is not reported, and relevant experimental details are not available to approximate the value. (Left-b) indicates the selectivity towards benzene production, taken from references indicated in (Left-a). * indicates that the reported selectivity is for C_6-C_{11} , and not solely C_6H_6 as for the other catalysts. (Center) shows the molecular structures of isolated MO_x within the 10 M rings of ZSM-5 support prior to MDA reaction. (Right) shows operando Raman spectroscopy, adapted from ref. 84 of the three best MDA catalysts Re \sim Mo > W, correlating the reducibility of the initial isolated metal oxide site with benzene light-off temperature. The $T_{\rm red}$ values pertain to the temperature where M \equiv O bond completely disappears and $T_{C_cH_c}$ values refer to temperature that benzene production is first observed.

supported group V-VIII oxide/ZSM-5 catalysts in Fig. 5(left-a) and benzene selectivity in Fig. 5(left-b). For the TOF calculation, the reported weight loading of the respective metal atoms was utilized from the original reports. 9,24 Although it is theoretically possible to back-calculate the TOF from literature reports if reaction conditions, kinetic parameters and metal oxide loadings are known, we caution the reader against it. TOF should only be calculated when only a single type of site is present, corroborated by molecular spectroscopy (Raman). For example, in a catalyst with a known Mo-loading, if a mixture of crystalline and dispersed phase Mo-sites are present, the CH₄ conversion or C₆H₆ production per Mo atom cannot be calculated accurately. Since Mo in crystalline MoO3 is not active for MDA but ZSM-5 confined Mo sites are, using theoretical Mo-loading will yield erroneous TOF values. Please see Table 2 and relevant discussion in the following sub-section.

Fig. 5(left-a) suggests that the supported ReO_x/ZSM-5 and MoO_x/ZSM-5 catalysts exhibit the highest benzene production TOF values amongst group V-VIII catalysts, with the supported

ReO_x/ZSM-5 catalyst just barely more active than MoO_x/ZSM-5. Although the specific activity of the supported ReO_r/ZSM-5 catalyst can be slightly higher than that of the supported MoO_r/ZSM-5 catalyst for the MDA reaction, the potential volatilization of ReO_x species during calcination, MDA reaction and catalyst regeneration compromises the practical use of supported ReO_x-based catalysts. MDA activity, which is indicated by the trend in TOF for benzene production over supported MO_x/ZSM-5 catalysts can be summarized as follows: $\text{ReO}_x/\text{ZSM-5} \sim \text{MoO}_x/\text{ZSM-5} > \text{WO}_x/\text{ZSM-5} \sim \text{FeO}_x/\text{ZSM-5} >$ $VO_x/ZSM-5 > CrO_x/ZSM-5$. Next, the selectivity to benzene is compared in Fig. 5(left-b) and shows that CrO_x/ZSM-5, MoO_x/ZSM-5 and FeO_x/ZSM-5 exhibit similar selectivity values of \sim 70-75%, WO_x/ZSM-5 and ReO_x/ZSM-5 \sim 50-55%, and $VO_x/ZSM-5 \sim 30\%$. Note that the reported selectivity in the case of $ReO_x/ZSM-5$ is for C_6-C_{11} , and not solely for C_6H_6 .

Structure-function (or nature-performance) relationships can be envisioned for the three most active catalysts (ReOx/ ZSM-5 \sim MoO_x/ZSM-5 > WO_x/ZSM-5) by correlating the *operando* **Review Article**

Table 2 MDA reaction performance of Mo/ZSM-5 catalysts reported in the literature. Parameters summarized in the table include Mo loading, catalyst synthesis techniques, Si/Al ratio, and total reaction pressure

Synthesis technique	Si/Al	Mo loading (wt%)	Reaction conditions			CH_4	C_6H_6	
			T (K)	P (kPa)	space velocity (ml g^{-1} cat ⁻¹ h^{-1})	conversion (%)	selectivity (%)	Ref.
Incipient-wetness impregnation of aqueous $(NH_4)_6Mo_7O_{24}\cdot 4H_2O$	50	1 2 3 4.5 6 8 10	973	115	1500	1.4 4.5 6.3 5.2 2.7 3.4 3.1	82 ^a 92.9 ^a 94.4 ^a 93.4 ^a 86.3 ^a 91.2 ^a 90 ^a	118
Incipient-wetness impregnation of aqueous $(NH_4)_6Mo_7O_{24}\cdot 4H_2O$	23	1 2 4 8 10	973	_	1500	4.5 6 12.5 9.5 8	_ _ _ _	119
Wetness impregnation of (NH ₄) ₆ Mo ₇ O ₂₄ ·4H ₂ O Wetness impregnation combined with treatment by rotavapor Wetness impregnation assisted by ultrasound treatment	20.4		973	101	3600	8 10.5	65 70 70	122
Wetness impregnation assisted by untrasound treatment Wetness impregnation assisted by microwave treatment Mechanical mixing of ZSM-5 with ammonium molybdate Impregnation of ammonium paramolybdate	25		1023	101	800^d	11 14.5 7 7.6 7.9 ^e	77 62 78.4 72.2	9
Solid state ion exchange of $MoCl_3$ with ZSM-5						2.6 7.5 ^e	71.5 71.2	
Incipient-wetness impregnation of aqueous (NH ₄) ₆ Mo ₇ O ₂₄ Solvothermal synthesis Solvothermal synthesis utilizing 10 v% ethanol/water	23	5	973	_	1500	12.5 13 15	38 46 33	120
as solvent Impregnation of $(NH_4)_6Mo_7O_{24}\cdot 4H_2O$	25 50	2	973	200	1440	7.2 4.4	100 100	8
Physical mixing of MoO ₃ and ZSM-5	15 25 40	2	1023	_	1500	18 ^c 22 ^c 22 ^c	67^{b} 30^{b} 32^{b}	123
Incipient wetness impregnation of (NH ₄) ₆ Mo ₇ O ₂₄ ·4H ₂ O	15 25 40	3	973	_	1550	8 ^c 6 ^c 3 ^c	70 60 45	121
Incipient-wetness impregnation of aqueous	17	2	993	_	1350	14 ^c	78	124
$(NH_4)_6Mo_7O_{24}\cdot 4H_2O$ Wetness impregnation of $(NH_4)_6Mo_7O_{24}\cdot 4H_2O$	13	2	973	20 50 100 200 300 400 600 800 1000 1500	15000^d	24.7 ^f 27.8 ^f 34.0 ^f 48.0 ^f 63.3 ^f 84.5 ^f 103.0 ^f 127.2 ^f 137.2 ^f 162.0 ^f	11.1 18.5 26.1 31.4 34.2 39.2 40.0 41.8 41.3 43.4	107

^a Selectivity of all aromatic products are reported. ^b C_6H_6 selectivity was back calculated from the knowledge of CH_4 conversion and C_6H_6 yield. ^c CH_4 conversion was taken at the maximum C_6H_6 selectivity. ^d Gas hourly space velocity: GHSV (h⁻¹) ^e Pretreated with CO at 773 K for 6 hours. ^f CH_4 conversion is given as mmol g^{-1} cat⁻¹. Average values were used for reproducible experiments.

Raman spectroscopy data available in the literature, 84 with the trend in TOF values reported in Fig. 5(left-a). For each catalyst, the initial molecular structure of the metal oxide site present within the 10 M ZSM ring is shown in Fig. 5(center). The *operando* Raman spectra Fig. 5(right) were used to track the diminishing M \Longrightarrow O bands as the metal oxide sites carburized with increasing MDA reaction time. $T_{\rm red}$ corresponds to the temperature that

M=O Raman bands completely vanished, while $T_{\rm C_6H_6}$ corresponds to the temperature that benzene was first detected in the MS. *Operando* Raman data suggests that the tri-oxo ReO₄/ZSM-5 sites (1013 cm⁻¹) reduced at 500 °C, followed by reduction of di-oxo MoO₄/ZSM-5 (993 cm⁻¹) at ~680–690 °C, and di-oxo WO₄/ZSM-5 (1024 cm⁻¹) at above 700 °C. Severe fluorescence was observed for the WO_x/ZSM-5 above 700 °C, making it hard to

ascertain the exact $T_{\rm red}$. Likewise, $T_{\rm C_eH_6}$ was 664, 781, and 814 $^{\circ}{\rm C}$ for ReO_x/ZSM-5, MoO_x/ZSM-5, and WO_x/ZSM-5 catalysts, respectively. The trends in reducibility of the initial dispersed phase, isolated metal oxide sites confined within the ZSM-5 pores, and the benzene production temperatures correlate strongly. In fact, for the Mo/ZSM-5 catalyst with well-defined MoO_x sites, experimental and computational study evidenced that differences in geometries and electronic properties of Mo carbide structures formed from distinct MoO_r anchored on Al and Si sites yielded differences in their catalytic properties.⁴² Specifically, the CH₄ activation energy over the Mo carbide anchored on the double Al-atom site was calculated to be 112 kJ mol^{-1} , while it was $\sim 140 \text{ kJ mol}^{-1}$ for the Mo carbide anchored on Si sites. 42 Therefore, special attention should be paid to synthesis and in-depth characterization of initial oxide forms of the ZSM-5 supported catalysts.

Factors affecting MDA performance of MoO_x/ZSM-5 catalysts

The relative performance comparison of various group V-VIII transition metal catalysts in the previous section shows that Mo-based catalysts exhibit high activity and stability. Hence, we further analyze various factors (material and process) that can affect the MDA performance of MoO_x/ZSM-5 catalysts. The literature reports that included pertinent experimental details are summarized in Table 2 along with key parameters. Table 2 highlights significant variability in MDA activity and selectivity of MoO_x/ZSM-5 catalysts across the literature. Nevertheless, the following general conclusions can be drawn from the comparison of data (CH₄ conversion and C₆H₆ selectivity) summarized in Table 2.

(a) Effect of Mo loading. The loading of Mo in supported MoO_x/ZSM-5 catalysts plays a crucial role in determining the catalyst's performance towards MDA reaction. The CH₄ conversion goes through a maximum with increasing Mo weight loading, reaches the maximum conversion at ~3-4 wt% loading, beyond which conversion drops. 118,119 This trend in CH₄ conversion can be related to the nature of the MoO_x sites in the catalyst. At low loading (From 0 to \sim 3-4 wt%), Mo-oxide is largely present as dispersed, isolated MoO_x sites confined within the zeolitic pores, which are known to be selective active sites for C-H activation. After 3-4% weight loading, further increase in the Mo content results in the formation of crystalline MoO₃ particles (nano- and micro scale) mostly on the external surface of the zeolite, which corresponds to the decreased CH4 activity. The maximum Mo loading beyond which MoO₃ NPs are formed, however, can be above 3-4 wt% in certain cases depending on the Al sites, which in turn depend on the Si/Al ratio of the ZSM-5 support. These crystalline MoO₃ are known to form coke on the external surface, which blocks the selective active sites within the zeolitic pores. Although carbided Mo sites are present during MDA reaction, the initial dispersion and structure of MoOx sites are crucial in determining the observed catalytic performance. On the other hand, the C₆H₆ selectivity exhibits a very low dependency on Mo loading. The selectivity value increases only slightly with Mo loading (up to 3-4 wt% loading) and remains approximately constant thereafter.

- (b) Effect of synthesis technique. Incipient wetness impregnation (IWI) of an aqueous solution of (NH₄)₆Mo₇O₂₄ into ZSM-5 support, followed by oxidative calcination is the most used synthesis technique for MoO_x/ZSM catalyst preparation. When done carefully, the IWI method can result in uniform dispersion of the MoO_r phase into the ZSM-5 support. The higher dispersion of MoOx species from IWI synthesis most likely responsible for the higher MDA activity of those catalysts compared to the ones synthesized via solid-state ion exchange of MoCl₃ or a mechanical mixing of MoO₃ with ZSM-5 support.⁹ In the latter synthesis method, residual crystalline MoO₃ nanoparticles are always present and adversely affect the MDA performance. Recently, novel synthesis approach of wetness impregnation assisted with additional treatment in rotavapor, microwave and ultrasound resulted in catalysts with appreciably higher MDA activity, tested up to 4 hours of time-onstream (TOS). Moreover, solvothermal synthesis utilizing 10 v% ethanol/water as solvent has also been reported to yield catalysts that were more active towards MDA compared to the IWI catalyst, tested up to 15 hours of TOS. 120 Catalysts synthesized using solvothermal approach were claimed to have a higher dispersion of the MoO_x sites on ZSM-5 in the freshly prepared catalysts. Having said that, additional catalyst characterization studies are required under in situ and operando conditions to corroborate the exact reason behind superior performance of catalysts prepared via advanced synthesis techniques instead of the traditional IWI. Additionally, one more investigation compared the effect of utilizing hexamolybdate [(C₄H₉)₄N]₂Mo₆O₁₉ vs. heptamolybdate (NH₄)₆Mo₇O₂₄·4H₂O as the Mo-oxide precursor and found that when hexamolybdate is used as precursor, the C₆H₆ selectivity is much improved.43
- (c) Effect of Si/Al ratio. The Si/Al ratio, which controls the acidity of the zeolite support and the dispersion of the supported metal oxide phase is a crucial parameter in MDA performance of MoO_x/ZSM-5 catalysts: higher acidity ZSM-5 support with low Si/Al ratio generally leads to a greater number of surface MoO_x sites and higher MDA activity. The literature converges on the understanding that higher the amount of Brønsted acid sites (i.e. low Si/Al ratio), higher the dispersion of isolated MoO_x sites within the zeolitic pores will be, which leads to superior MDA activity from the dispersed Mo sites confined within the ZSM-5 pores.8,121 This trend further highlights the relevance of characterizing and understanding the nature of dispersed phase sites in MDA catalysts.
- (d) Effect of reaction pressure. Only a limited number of studies have undertaken examining the effect of reaction pressure on the MDA performance of MoO_x/ZSM-5 catalyst. Recently, it was reported that with increasing reaction pressure, both CH₄ conversion and C₆H₆ selectivity values increase. 107 The positive effect of higher reaction pressure towards MDA performance was attributed to the decrease in coke formation/ catalyst deactivation rate. Higher pressure aiding MDA kinetics was surprising, as higher pressures are expected to shift the reaction towards the reactant's side, given the stoichiometry of 6 moles of CH4 reactant forming 10 moles of product (1 benzene, 9 hydrogen).

6. Kinetics and reaction mechanism of MDA over supported $MO_x/ZSM-5$ catalysts

Rate-determining-step (RDS)

Review Article

The energy associated with the breaking of the C–H bond in the methane molecule ($\sim 437 \pm 2$ kJ mol $^{-1}$) 3,125,126 is extremely high. Such a large energetic barrier requires high temperatures to initiate C–H bond activation, especially for the non-oxidative conversion of methane. The C–H bond breaking of CH₄ is, therefore, generally considered the rate-determining-step in methane chemical reactions. Temperature programmed MDA studies with the CH₄ and CD₄ isotopes demonstrated a significant kinetic isotope effect ($T_{\rm p} = 890$ K for CH₄ and $T_{\rm p} = 1042$ K for CD₄) establishing that breaking of the C–H bond of methane is indeed the rate-determining-step. The section of the condition of th

Most abundant reaction intermediate (MARI)

Given that the RDS is the activation of the C–H bond upon adsorption of $\mathrm{CH_4}$, all subsequent reaction steps will be extremely fast. This is confirmed by the immediate production of benzene and hydrogen over an activated catalyst (*i.e.*, when the induction period is over). Consequently, the population of surface reaction intermediates will be negligible under MDA reaction conditions and difficult to detect spectroscopically. Gas-phase methyl radicals are also generated and their contribution to the MDA reaction must be quantified, but no such reports have appeared to date. ³⁹

Many studies have proposed ethylene and acetylene as the primary reaction intermediates for the MDA reaction. 39,127 One of the reasons cited for identifying ethylene and acetylene as reaction intermediates is that benzene is formed upon dosing either of these C2 hydrocarbons over supported MOx/ZSM-5 catalysts. The feeding of ethylene generally produces higher selectivity for toluene, whereas acetylene (as a feed) results in similar selectivity towards toluene and benzene, compared to that of methane. Moreover, the more reactive acetylene molecule exhibited higher benzene formation rates than ethylene. 99,108,112 It was also shown that acetylene was not observed as a side-product of the MDA reaction, possibly due to its high reactivity. Acetylene easily hydrogenates to ethylene in the presence of hydrogen, which may explain why some authors observed ethylene during MDA while a few observed acetylene. 128 To circumvent the gas-phase reactions of the acetylene intermediate, recently, low residence times in conjunction with microwave heating instead of conventional (resistive) heating, were used to establish a gas-solid temperature gradient provided by the selective heating and the low gas-solid contact time. 129 This approach apparently quenched gas-phase reactions and enabled detection of the acetylene and carbon monoxide intermediates in appreciable quantities. Over the same catalyst, acetylene was not detected using conventional heating reactor. 129 On the other hand, a recent report has cast doubt on ethylene being the primary intermediate. 127 It was concluded that ethylene was not the major reaction intermediate because the hydrocarbon pool formed in the

zeolite matrix during MDA is comprised of less dense and more hydrogenated species than the pool formed from ethylene. Moreover, the carbonaceous deposits formed from methane were also more reactive than the ones formed from ethylene. As mentioned above, the RDS is the cleavage of the C–H bond of CH₄ and, consequently, it is highly unlikely that reaction intermediates can be detected *via* conventional approaches because all steps after the RDS are expected to be extremely fast (especially at/above 973 K).

MDA reaction mechanism

The exact MDA mechanism remains under debate. Literature reports corroborating opposing proposals are available: (1) monofunctional mechanism with Mo sites being solely responsible for all catalytic steps, ^{99,112} and (2) bi-functional mechanism where Mo sites activate CH₄ and adjacent framework Brønsted acid sites polymerize and aromatize the C₂ intermediates. ^{130–132} The majority of MDA studies with supported Mo/ZSM-5, the most investigated MDA catalyst, reported that the Mo-carbide sites within the pores were responsible for the activation of C-H bond in methane and converting the CH_r intermediates into ethylene/acetylene. Subsequently, the ethylene/acetylene oligomerization and aromatization to benzene and other aromatic products was proposed to occur on the framework Brønsted acid sites in the zeolite micropores. 130-132 Alternatively, the mono-functional mechanism^{99,107,112} proposes that both the activation of methane and subsequent reaction of the hydrocarbon pool to benzene exclusively occurs at Mo carbide sites. 127,133,134 It was recently reported that the supported MO_xC_y/silicalite-1 catalyst, which doesn't contain Brønsted acidity and has the same topology as ZSM-5, was able to convert methane into benzene and aromatic coke at 973 K. It was, therefore, inferred that framework Brønsted acid sites were not required for MDA and that the conversion of methane to benzene followed a monofunctional mechanism on highly dispersed Mo carbide species embedded in the 10MR zeolite micropores. 112 The lower catalytic performance of MO_xC_y/silicalite-1 catalyst compared to the Mo/ZSM-5 catalyst was attributed to the lack of Brønsted acid sites that aid in stabilizing and dispersing both the initial MoO_r and MO_xC_y active sites inside the zeolite pores. The presence of the hydrocarbon pool and hydrocarbon pool mechanism was experimentally verified by pulsing isotopically labelled CH₄ (13CH₄, CD₄). 99,111 A recent computational study also determined that, at least over MO_xC_v sites, the radical hydrocarbon-pool pathway was energetically less demanding and, thus, more favorable. 135 Currently, the exact mechanism of how the radical hydrocarbonpool forms and cooperates during MDA to form benzene is not understood and requires further probing using operando spectroscopy studies with high spatial and temporal resolution. 108

7. $MoO_x/ZSM-5$ catalyst's stability and deactivation under MDA

It is well known that ZSM-5 supported MDA catalysts experience systematic deactivation with time on stream due to coke formation leading to pore blockage, and due to larger MoO_x

clusters at the external surface sintering at elevated temperature during reaction. Previously, process-intensification strategies have been proposed to circumvent the catalyst deactivation, which include cycling H2 feed after CH4 to reactivate the catalyst, 120 increasing the reaction pressure to 15 bar to speed up hydrogenation of deposited coke, 107 O2-treatment to reverse both the carbide formation and the agglomeration of Mo nanostructures to regenerate the deactivated catalyst, 42 and using low temperature H₂-pre-reduction before carburization to form a higher population of dispersed MO_xC_y species. 136 The state-of-the art understanding regarding coking of Mo/ZSM-5 catalysts during reaction is that graphite-like external coke is more detrimental to the activity of the catalyst than internal coke. 135 External coke formation leads to blockage of the pore openings, which in turn decreases the access of CH₄ to the zeolite channels. 135

Chem Soc Rev

A noteworthy synthesis approach, aimed at improving Mo/ZSM-5 catalyst's stability, utilizes continuous solvothermal synthesis method under supercritical conditions and reducing atmosphere to synthesize 5% Mo/ZSM-5.¹²⁰ Although lacking in situ or operando characterization of their material, the study boasts an impressive stable performance of the catalyst for ~15 hours on stream. The authors attributed enhanced stability of the catalyst prepared via the novel synthesis route to delayed formation of detrimental so-called hard coke species. 120 Very recently, however, 0.5%Mo was successfully loaded onto nano ZSM-5 to yield a single site Mo/ZSM-5 catalyst in contrast to a mixture of Mo phases typically present in traditionally prepared Mo/ZSM-5 catalysts. 137 This novel nano Mo/ZSM-5 material was shown be to orders of magnitude more stable than regular Mo/ZSM-5 catalysts, with the longest time on stream of 36 hours (3 cycles \times 12 hours each), without an appreciable decrease in CH₄ conversion. 137 However, minor dealumination occurred in the material during multiple cycles, as evidenced by a decrease in unit cell volume. 137 Note that the degree of dealumination observed in this nano Mo/ZSM-5 catalyst was minuscule compared to that observed in traditionally prepared 1% Mo/ZSM-5 catalyst. It suffices to say that while this ultra-stable nano Mo/ZSM-5 synthesis approach has significantly improved the catalyst stability, various other synthetic approaches to impart greater stability found in zeolite-synthesis literature include encapsulation of metal ions/atoms during zeolite crystallization, 138 alkalistabilized metal incorporation into zeolite pores, 139 stabilization of extra framework sites via substituted framework atoms to exploit strong-metal-support-interaction (SMSI) phenomena, 140-142 etc. An excellent, state-of-the-art review of the various strategies to improve zeolite-based catalysts' stability towards prolonged operation under harsh reaction conditions, similar to those required for MDA, can be found elsewhere in the literature. 143

8. Summary and outlook

There are still disagreements in the literature of MDA catalysis of supported MO_x/ZSM-5 catalysts primarily because of information gaps, despite a large number of publications on the topic. While the nature of the dispersed MO_x sites is much

better understood for the group VI metal oxides in supported MO_x/ZSM-5 catalysts (Cr, Mo, W), more research is still needed for the ZSM-5 supported group V(V)-, group VII(Re)- and group VIII(Fe)-containing catalysts. Under MDA reaction conditions, the initially dispersed, fully oxidized MO_x sites become reduced to oxycarbide and carbide clusters that represent the catalytic active sites. The surface ReOx site becomes reduced to metallic Re⁰. The rds is the breaking of the C-H bond during the CH₄ adsorption step, which makes all subsequent steps kinetically insignificant. In terms of catalytic MDA performance, the supported MoO_x/ZSM-5 catalyst system appears to be the best candidate amongst all of the group V-VIII metal oxides discussed herein. With regards to the reaction mechanism, the literature leans towards the radical hydrocarbon pool mechanism proceeding with activation and aromatization at mono-functional metal carbide cluster sites. Considerable research on supported MO_x/ZSM-5 catalysts for MDA is expected in the coming years to address both the unresolved fundamental issues (molecular structures of the dehydrated surface MO_x sites, anchoring sites of the surface MO_x sites on the ZSM-5 support, and nature of catalytic active sites under MDA reaction conditions) and applied aspects (increasing benzene yield and deactivation from coking).

Further advancement of the fundamental structure-activity relationships of the MDA catalytic reaction using group V-VIII MOx-based ZSM-5 catalysts to guide the rational design and optimization of these catalysts for MDA will require the following:

- Isotopic 18O2-16O2 exchange in situ Raman studies to determine the number of terminal M=O oxo bonds present for all the dehydrated surface MO_x sites on the ZSM-5 support.
- Operando Raman and XAS spectroscopy studies to completely understand the molecular structures of the catalytic active sites under the MDA reaction conditions.
- Complementary operando Near Atmospheric Pressure (NAP)-XPS, UV-vis DRS, and XAS studies to provide information about the oxidation states of the catalytic active sites during MDA.
- · Modulation excitation spectroscopy (MES) and isotopeswitch experiments to elucidate the nature of the reaction intermediates and reaction network.
- Operando photoelectron photoion coincidence spectroscopy (PEPICO)144 and online synchrotron vacuum ultraviolet photoionization mass spectroscopy (SVUV-PIMS)145 to provide information on the involvement of gas-phase radical species in the MDA mechanism.
- Operando UV-Vis analysis of carefully synthesized, oriented ZSM-5-based catalysts have recently shown the ability to unravel structure-function relationships by elucidating chemistries occurring within the zeolite pores versus the external surface. 146

Conflicts of interest

There are no conflicts to declare.

Acknowledgements

This work was supported by NSF CBET Award #1706581. All authors have read and agreed to the final version of the manuscript.

Review Article Chem Soc Rev

References

- 1 T. Mokrani and M. Scurrell, Catal. Rev., 2009, 51, 1-145.
- 2 M. B. Park, E. D. Park and W.-S. Ahn, Front. Chem., 2019, 7, 514.
- 3 D. Kiani, S. Sourav, J. Baltrusaitis and I. E. Wachs, *ACS Catal.*, 2019, **9**, 5912–5928.
- 4 D. Kiani, S. Sourav, W. Taifan, M. Calatayud, F. Tielens, I. E. Wachs, J. Baltrusaitis, I. E. Wachs and J. Baltrusaitis, ACS Catal., 2020, 10, 4580-4592.
- 5 D. Kiani, S. Sourav, I. E. Wachs and J. Baltrusaitis, *Catal. Sci. Technol.*, 2020, **10**, 3334–3345.
- 6 Y. Gao, L. Neal, D. Ding, W. Wu, C. Baroi, A. M. Gaffney and F. Li, ACS Catal., 2019, 9, 8592–8621.
- 7 B. M. Weckhuysen, D. Wang, M. P. Rosynek and J. H. Lunsford, *J. Catal.*, 1998, 175, 347–351.
- 8 L. Wang, L. Tao, M. Xie, G. Xu, J. Huang and Y. Xu, Catal. Lett., 1993, 21, 35-41.
- 9 B. M. Weckhuysen, D. Wang, M. P. Rosynek and J. H. Lunsford, J. Catal., 1998, 175, 338–346.
- 10 J. Hao, P. Schwach, G. Fang, X. Guo, H. Zhang, H. Shen, X. Huang, D. Eggart, X. Pan and X. Bao, *ACS Catal.*, 2019, 9, 9045–9050.
- 11 M. Sakbodin, Y. Wu, S. C. Oh, E. D. Wachsman and D. Liu, *Angew. Chem., Int. Ed.*, 2016, 55, 16149–16152.
- 12 M. Moser, L. Rodríguez-García, A. P. Amrute and J. Pérez-Ramírez, *ChemCatChem*, 2013, 5, 3520–3523.
- 13 V. Paunović, G. Zichittella, M. Moser, A. P. Amrute and J. Pérez-Ramírez, *Nat. Chem.*, 2016, 8, 803–809.
- 14 G. Zichittella, V. Paunović, A. P. Amrute and J. Pérez-Ramírez, ACS Catal., 2017, 7, 1805–1817.
- 15 J. Tollefson, "Flaring" wastes 3.5% of world's natural gas.
- 16 Zero Routine Flaring by 2030, https://www.worldbank.org/en/programs/zero-routine-flaring-by-2030#1.
- 17 M. Wark, A. Brückner, T. Liese and W. Grünert, *J. Catal.*, 1998, 175, 48–61.
- 18 Y. F. Chang, G. A. Somorjai and H. Heinemann, *J. Catal.*, 1995, **154**, 24–32.
- 19 A. de Lucas, J. L. Valverde, L. Rodriguez, P. Sanchez and M. T. Garcia, *Appl. Catal.*, A, 2000, 203, 81–90.
- 20 T. K. Katranas, K. S. Triantafyllidis, A. G. Vlessidis and N. P. Evmiridis, in *Oxide Based Materials*, ed. A. Gamba, C. Colella and S. Coluccia, Elsevier, 2005, vol. 155, pp. 347–354.
- 21 P. K. Chaudhari, P. K. Saini and S. Chand, *J. Sci. Ind. Res.*, 2002, **61**, 810–816.
- 22 A. Z. Abdullah, M. Z. A. Bakar and S. Bhatia, *Catal. Commun.*, 2003, 4, 555–560.
- 23 A. Z. Abdullah, M. Z. Abu Bakar and S. Bhatia, *Ind. Eng. Chem. Res.*, 2003, **42**, 6059–6067.
- 24 H. S. Lacheen, P. J. Cordeiro and E. Iglesia, *Chem. Eur. J.*, 2007, **13**, 3048–3057.
- 25 Y. Traa, B. Burger and J. Weitkamp, *Microporous Meso-porous Mater.*, 1999, **30**, 3-41.
- 26 N. Mimura, I. Takahara, M. Inaba, M. Okamoto and K. Murata, *Catal. Commun.*, 2002, 3, 257–262.
- 27 H. Yamashita, S. Ohshiro, K. Kida, K. Yoshizawa and M. Anpo, *Res. Chem. Intermed.*, 2003, **29**, 881–890.

- 28 M. E. Swanson, H. L. Greene and S. Qutubuddin, *Appl. Catal.*, B, 2004, 52, 91–108.
- 29 F. Solymosi and P. Tolmacsov, Catal. Lett., 2004, 93, 7-11.
- 30 N. A. S. Amin and S. E. Pheng, *Catal. Commun.*, 2006, 7, 403–407.
- 31 W. Ding, G. D. Meitzner, D. O. Marler and E. Iglesia, J. Phys. Chem. B, 2001, 105, 3928–3936.
- 32 J. A. Biscardi, G. D. Meitzner and E. Iglesia, *J. Catal.*, 1998, **179**, 192–202.
- 33 Y. Xu, M. Chen, T. Wang, B. Liu, F. Jiang and X. Liu, J. Catal., 2020, 387, 102–118.
- 34 Y. Xu, M. Chen, B. Liu, F. Jiang and X. Liu, *Chem. Commun.*, 2020, **56**, 4396–4399.
- 35 O. V. Bragin, T. V. Vasina, A. V. Preobrazhenskii and K. M. Minachev, Bull. Acad. Sci. USSR, Div. Chem. Sci., 1989, 38, 680.
- 36 O. V. Bragin, T. V. Vasina, Y. I. Isakov, B. K. Nefedov, A. V. Preobrazhenskii, N. V. Palishkina and K. M. Minachev, Bull. Acad. Sci. USSR, Div. Chem. Sci., 1982, 31, 847.
- 37 O. V. Bragin, A. V. Preobrazhenskii and A. L. Liberman, Bull. Acad. Sci. USSR, Div. Chem. Sci., 1974, 23, 1599.
- 38 K. Sun, D. M. Ginosar, T. He, Y. Zhang, M. Fan and R. Chen, *Ind. Eng. Chem. Res.*, 2018, 57, 1768–1789.
- 39 I. Vollmer, I. Yarulina, F. Kapteijn and J. Gascon, *Chem-CatChem*, 2019, 11, 39–52.
- 40 J. J. Spivey and G. Hutchings, Chem. Soc. Rev., 2014, 43, 792–803.
- 41 S. Ma, X. Guo, L. Zhao, S. Scott and X. Bao, *J. Energy Chem.*, 2013, 22, 1–20.
- 42 J. Gao, Y. Zheng, J. M. Jehng, Y. Tang, I. E. Wachs and S. G. Podkolzin, *Science*, 2015, 348, 686–690.
- 43 I. Julian, J. L. Hueso, N. Lara, A. Solé-Daurá, J. M. Poblet, S. G. Mitchell, R. Mallada and J. Santamaría, *Catal. Sci. Technol.*, 2019, 9, 5927–5942.
- 44 R. W. Borry, Y. H. Kim, A. Huffsmith, J. A. Reimer and E. Iglesia, J. Phys. Chem. B, 1999, 103, 5787–5796.
- 45 W. Li, G. D. Meitzner, R. W. Borry and E. Iglesia, *J. Catal.*, 2000, **191**, 373–383.
- 46 H. S. Lacheen and E. Iglesia, *J. Phys. Chem. B*, 2006, **110**, 5462–5472.
- 47 M. Petráš, B. Wichterlová, M. Petras and B. Wichterlova, J. Phys. Chem., 1992, 96, 1805–1809.
- 48 F. Ayari, M. Mhamdi, D. P. Debecker, E. M. Gaigneaux, J. Alvarez-Rodriguez, A. Guerrero-Ruiz, G. Delahay and A. Ghorbel, J. Mol. Catal. A: Chem., 2011, 339, 8–16.
- 49 J. Gao, Y. Zheng, Y. Tang, J. M. Jehng, R. Grybos, J. Handzlik, I. E. Wachs and S. G. Podkolzin, ACS Catal., 2015, 5, 3078–3092.
- 50 H. Liu, W. Shen, X. Bao and Y. Xu, J. Mol. Catal. A: Chem., 2006, 244, 229–236.
- 51 I. Vollmer, G. Li, I. Yarulina, N. Kosinov, E. J. Hensen, K. Houben, D. Mance, M. Baldus, J. Gascon and F. Kapteijn, *Catal. Sci. Technol.*, 2018, 8, 916–922.
- 52 W. Liu and Y. Xu, J. Catal., 1999, 185, 386-392.
- 53 D. Wang, J. H. Lunsford and M. P. Rosynek, *J. Catal.*, 1997, 169, 347–358.

54 R. G. Bell, R. A. Jackson and C. R. A. Catlow, Zeolites, 1992, **12**, 870-871.

Chem Soc Rev

- 55 V. Pashkova, P. Klein, J. Dedecek, V. Tokarová and B. Wichterlová, Microporous Mesoporous Mater., 2015, 202,
- 56 Y. Zheng, Y. Tang, J. R. Gallagher, J. Gao, T. Miller, I. E. Wachs and S. G. Podkolzin, J. Phys. Chem. C, 2019, 123, 22281-22292.
- 57 M. Agote-Arán, A. B. Kroner, H. U. Islam, W. A. Sławiński, D. S. Wragg, I. Lezcano-González and A. M. Beale, ChemCatChem, 2019, 11, 473-480.
- 58 Z.-T. Xiong, H.-B. Zhang, G.-D. Lin and J.-L. Zeng, Catal. Lett., 2001, 74, 233-239.
- 59 H. S. Lacheen, P. J. Cordeiro and E. Iglesia, J. Am. Chem. Soc., 2006, 128, 15082-15083.
- 60 Y. Wu, S. Holdren, Y. Zhang, S. C. Oh, D. T. Tran, L. Emdadi, Z. Lu, M. Wang, T. J. Woehl, M. Zachariah, Y. Lei and D. Liu, J. Catal., 2019, 372, 128-141.
- 61 M. A. Vuurman and I. E. Wachs, J. Phys. Chem., 1992, 96, 5008-5016.
- 62 M. A. Vuurman, D. J. Stufkens, A. Oskam and I. E. Wachs, J. Mol. Catal., 1992, 76, 263-285.
- 63 S. Lwin, C. Keturakis, J. Handzlik, P. Sautet, Y. Li, A. I. Frenkel, I. E. Wachs, A. I. Frenkel, I. E. Wachs, A. I. Frenkel and I. E. Wachs, ACS Catal., 2015, 5, 1432-1444.
- 64 S. Lwin, Y. Li, A. I. Frenkel and I. E. Wachs, ACS Catal., 2015, 5, 6807-6814.
- 65 H.-Y. Chen and W. M. H. Sachtler, Catal. Today, 1998, 42, 73-83.
- 66 P. Marturano, L. Drozdová, A. Kogelbauer and R. Prins, J. Catal., 2000, 192, 236-247.
- 67 G. Wu, F. Hei, N. Zhang, N. Guan, L. Li and W. Grünert, Appl. Catal., A, 2013, 468, 230-239.
- 68 M. P. McDaniel, in Advances in Catalysis, ed. D. D. Eley, H. Pines and P. B. Weisz, Academic Press, 1985, vol. 33, pp. 47-98.
- 69 C. Moisii, E. W. Deguns, A. Lita, S. D. Callahan, L. J. van de Burgt, D. Magana and A. E. Stiegman, Chem. Mater., 2006, 18, 3965-3975.
- 70 B. M. Weckhuysen and I. E. Wachs, J. Phys. Chem. B, 1997, 101, 2793-2796.
- 71 D. K. Pappas, K. Kvande, M. Kalyva, M. Dyballa, K. A. Lomachenko, B. Arstad, E. Borfecchia, S. Bordiga, U. Olsbye, P. Beato and S. Svelle, Catal. Today, 2020, DOI: 10.1016/j.cattod.2020.06.050.
- 72 K. Yoshizawa and Y. Shiota, J. Am. Chem. Soc., 2006, 128, 9873-9881.
- 73 M. A. Newton, A. J. Knorpp, V. L. Sushkevich, D. Palagin and J. A. van Bokhoven, Chem. Soc. Rev., 2020, 49, 1449-1486.
- 74 A. v. Kucherov and A. A. Slinkin, J. Mol. Catal., 1994, 90,
- 75 A. V. Kucherov and A. A. Slinkin, Zeolites, 1987, 7, 38-42.
- 76 E. Gillis and E. Boesman, Phys. Status Solidi B, 1966, 14, 337-347.

- 77 C. Moisii, L. J. van de Burgt and A. E. Stiegman, Chem. Mater., 2008, 20, 3927-3935.
- 78 E. L. Lee, I. E. Wachs, E. L. Lee and I. E. Wachs, J. Phys. Chem. C, 2007, 111, 14410-14425.
- 79 X. Gao, S. R. Bare, B. M. Weckhuysen and I. E. Wachs, I. Phys. Chem. B, 1998, 102, 10842-10852.
- 80 K. Nakamoto, Infrared and Raman Spectra of Inorganic and Coordination Compounds, John Wiley & Sons, Ltd, 6th edn, 1988, vol. 92.
- 81 T. Tanaka, H. Yamashita, R. Tsuchitani, T. Funabiki and S. Yoshida, J. Chem. Soc., Faraday Trans. 1, 1988, 84, 2987-2999.
- 82 E. L. Lee and I. E. Wachs, Silica and Silicates in Modern Catalysis, 2010, pp. 375-404.
- 83 X. Gao and I. E. Wachs, J. Phys. Chem. B, 2000, 104, 1261-1268.
- 84 Y. Tang, 2014. "Nature of Catalytic Active Sites in Supported MOx/ZSM-5 Catalysts: Anchoring Sites, Electronic Structures, Molecular Structures and Reactivity" (2014). Theses and Dissertations. 2835. https://preserve.lehigh.edu/ etd/2835.
- 85 C. A. Carrero, R. Schloegl, I. E. Wachs and R. Schomaecker, ACS Catal., 2014, 4, 3357-3380.
- 86 N. R. Jaegers, C. Wan, M. Y. Hu, M. Vasiliu, D. A. Dixon, E. Walter, I. E. Wachs, Y. Wang and J. Z. Hu, J. Phys. Chem. C, 2017, 121, 6246-6254.
- 87 B. Wichterlová, Z. Tvarůžková and J. Nováková, J. Chem. Soc., Faraday Trans. 1, 1983, 79, 1573-1583.
- 88 N. Mimura, M. Okamoto, H. Yamashita, S. Ted Oyama and K. Murata, J. Phys. Chem. B, 2006, 110, 21764-21770.
- 89 R. Rachapudi, P. S. Chintawar and H. L. Greene, J. Catal., 1999, **185**, 58-72.
- 90 A. Müller, K. H. Schmidt, E. Ahlborn and C. J. L. Lock, Spectrochim. Acta, Part A, 1973, 29, 1773-1788.
- 91 E. L. Lee and I. E. Wachs, J. Phys. Chem. C, 2008, 112, 6487-6498.
- 92 Y. Yu, G. Xiong, C. Li and F.-S. Xiao, Microporous Mesoporous Mater., 2001, 46, 23-34.
- 93 P. K. Dutta and M. Puri, J. Phys. Chem., 2002, 91, 4329-4333.
- 94 A. M. Rzhevskii, P. Choi, F. H. Ribeiro, R. J. Gulotty and M. M. Olken, Catal. Lett., 2001, 73, 187-191.
- 95 H. Tian, I. E. Wachs and L. E. Briand, J. Phys. Chem. B, 2005, 109, 23491-23499.
- 96 A. Chakrabarti and I. E. Wachs, ACS Catal., 2018, 8, 949-959.
- 97 H. Tian, C. A. Roberts and I. E. Wachs, J. Phys. Chem. C, 2010, 114, 14110-14120.
- 98 I. Lezcano-González, R. Oord, M. Rovezzi, P. Glatzel, S. W. Botchway, B. M. Weckhuysen and A. M. Beale, Angew. Chem., Int. Ed., 2016, 55, 5215-5219.
- 99 N. Kosinov, A. S. G. Wijpkema, E. Uslamin, R. Rohling, F. J. A. G. Coumans, B. Mezari, A. Parastaev, A. S. Poryvaev, M. V. Fedin, E. A. Pidko and E. J. M. Hensen, Angew. Chem., 2018, 130, 1028-1032.
- 100 E. I. Ross-Medgaarden and I. E. Wachs, J. Phys. Chem. C, 2007, 111, 15089-15099.

101 E. I. Ross-Medgaarden, W. v. Knowles, T. Kim, M. S. Wong, W. Zhou, C. J. Kiely and I. E. Wachs, *J. Catal.*, 2008, 256, 108–125.

Review Article

- 102 D. S. Kim, M. Ostromecki and I. E. Wachs, J. Mol. Catal. A: Chem., 1996, 106, 93–102.
- 103 I. E. Wachs, T. Kim and E. I. Ross, *Catal. Today*, 2006, **116**, 162–168.
- 104 D. Kiani, G. Belletti, P. Quaino, F. Tielens and J. Baltrusaitis, J. Phys. Chem. C, 2018, 122, 24190–24201.
- 105 H.-Y. Chen, E.-M. El-Malki, X. Wang, R. A. van Santen and W. M. H. Sachtler, *J. Mol. Catal. A: Chem.*, 2000, 162, 159–174.
- 106 I. Vollmer, S. Ould-Chikh, A. Aguilar-Tapia, G. Li, E. Pidko, J.-L. Hazemann, F. Kapteijn and J. Gascon, J. Am. Chem. Soc., 2019, 141, 18814–18824.
- 107 N. Kosinov, E. A. Uslamin, L. Meng, A. Parastaev, Y. Liu and E. J. M. Hensen, *Angew. Chem., Int. Ed.*, 2019, 58, 7068–7072.
- 108 G. Li, I. Vollmer, C. Liu, J. Gascon and E. A. Pidko, ACS Catal., 2019, 9, 8731–8737.
- 109 I. Vollmer, N. Kosinov, Á. Szécsényi, G. Li, I. Yarulina, E. Abou-Hamad, A. Gurinov, S. Ould-Chikh, A. Aguilar-Tapia, J.-L. Hazemann, E. Pidko, E. Hensen, F. Kapteijn and J. Gascon, J. Catal., 2019, 370, 321–331.
- 110 I. Vollmer, B. van der Linden, S. Ould-Chikh, A. Aguilar-Tapia, I. Yarulina, E. Abou-Hamad, Y. G. Sneider, A. I. Olivos Suarez, J.-L. Hazemann, F. Kapteijn and J. Gascon, *Chem. Sci.*, 2018, 9, 4801–4807.
- 111 N. Kosinov, E. A. Uslamin, F. J. A. G. Coumans, A. S. G. Wijpkema, R. Y. Rohling and E. J. M. Hensen, *ACS Catal.*, 2018, **8**, 8459–8467.
- 112 N. Kosinov, F. J. A. G. Coumans, E. A. Uslamin, A. S. G. Wijpkema, B. Mezari and E. J. M. Hensen, *ACS Catal.*, 2016, 7, 520–529.
- 113 V. v Kozlov, V. I. Zaikovskii, A. v Vosmerikov, L. L. Korobitsyna and G. v Echevskii, *Kinet. Catal.*, 2008, **49**, 110–114.
- 114 C. J. Keturakis, M. Zhu, E. K. Gibson, M. Daturi, F. Tao, A. I. Frenkel and I. E. Wachs, ACS Catal., 2016, 6, 4786-4798.
- 115 M. Zhu and I. E. Wachs, ACS Catal., 2016, 6, 1764-1767.
- 116 M. Zhu and I. E. Wachs, ACS Catal., 2016, 6, 722-732.
- 117 B. M. Weckhuysen, D. Wang, P. Michael and J. H. Lunsford, *Angew. Chem., Int. Ed. Engl.*, 1997, **36**, 2374–2376.
- 118 Y. Xu, W. Liu, S.-T. Wong, L. Wang and X. Guo, *Catal. Lett.*, 1996, **40**, 207–214.
- 119 A. López-Martín, A. Caballero and G. Colón, *Mol. Catal.*, 2020, 486, 110787.
- 120 I. Julian, M. B. Roedern, J. L. Hueso, S. Irusta, A. K. Baden, R. Mallada, Z. Davis and J. Santamaria, *Appl. Catal., B*, 2020, 263, 118360.
- 121 M. Rahman, A. Infantes-Molina, A. S. Hoffman, S. R. Bare, K. L. Emerson and S. J. Khatib, *Fuel*, 2020, **278**, 118290.
- 122 K. Velebná, M. Horňáček, V. Jorík, P. Hudec, M. Čaplovičová and L. Čaplovič, *Microporous Mesoporous Mater.*, 2015, 212, 146–155.

- 123 J.-P. Tessonnier, B. Louis, S. Rigolet, M. J. Ledoux and C. Pham-Huu, *Appl. Catal.*, *A*, 2008, 336, 79–88.
- 124 E. v Matus, I. Z. Ismagilov, O. B. Sukhova, V. I. Zaikovskii, L. T. Tsikoza, Z. R. Ismagilov and J. A. Moulijn, *Ind. Eng. Chem. Res.*, 2007, 46, 4063–4074.
- 125 D. Wolf, Angew. Chem., Int. Ed., 1999, 37, 3351-3353.
- 126 P. Schwach, X. Pan and X. Bao, *Chem. Rev.*, 2017, **117**, 8497–8520.
- 127 I. Vollmer, E. Abou-Hamad, J. Gascon and F. Kapteijn, *ChemCatChem*, 2020, **12**, 544–549.
- 128 P. Tsai and J. R. Anderson, J. Catal., 1983, 80, 207-214.
- 129 I. Julian, H. Ramirez, J. L. Hueso, R. Mallada and J. Santamaria, *Chem. Eng. J.*, 2019, 377, 119764.
- 130 K. S. Wong, J. W. Thybaut, E. Tangstad, M. W. Stöcker and G. B. Marin, *Microporous Mesoporous Mater.*, 2012, **164**, 302–312.
- 131 C. Karakaya, H. Zhu and R. J. Kee, *Chem. Eng. Sci.*, 2015, **123**, 474–486.
- 132 M. C. Iliuta, I. Iliuta, B. P. A. Grandjean and F. Larachi, *Ind. Eng. Chem. Res.*, 2003, **42**, 3203–3209.
- 133 P. Mériaudeau, L. V. Tiep, V. T. T. T. Ha, C. Naccache and G. Szabo, *J. Mol. Catal. A: Chem.*, 1999, **144**, 469–471.
- 134 P. Mériaudeau, V. T. T. Ha and L. van Tiep, *Catal. Lett.*, 2000, **64**, 49–51.
- 135 X. Huang, X. Jiao, M. Lin, K. Wang, L. Jia, B. Hou and D. Li, *Catal. Sci. Technol.*, 2018, **8**, 5740–5749.
- 136 M. Rahman, A. Infantes-Molina, A. Boubnov, S. R. Bare, E. Stavitski, A. Sridhar and S. J. Khatib, *J. Catal.*, 2019, 375, 314–328.
- 137 S. v. Konnov, F. Dubray, E. B. Clatworthy, C. Kouvatas, J. P. Gilson, J. P. Dath, D. Minoux, C. Aquino, V. Valtchev, S. Moldovan, S. Koneti, N. Nesterenko and S. Mintova, *Angew. Chem.*, 2020, 59, 19553–19560, DOI: 10.1002/ange. 202006524.
- 138 L. Liu, U. Díaz, R. Arenal, G. Agostini, P. Concepción and A. Corma, *Nat. Mater.*, 2017, **16**, 132–138.
- 139 M. Yang, S. Li, Y. Wang, J. A. Herron, Y. Xu, L. F. Allard, S. Lee, J. Huang, M. Mavrikakis and M. Flytzani-Stephanopoulos, *Science*, 2014, **346**, 1498–1501.
- 140 Z. Xu, Y. Yue, X. Bao, Z. Xie and H. Zhu, ACS Catal., 2020, 10, 818–828.
- 141 Y. Wang, Z.-P. Hu, W. Tian, L. Gao, Z. Wang and Z.-Y. Yuan, *Catal. Sci. Technol.*, 2019, **9**, 6993–7002.
- 142 R. Ryoo, J. Kim, C. Jo, S. W. Han, J.-C. Kim, H. Park, J. Han, H. S. Shin and J. W. Shin, *Nature*, 2020, 585, 221–224.
- 143 E. B. Clatworthy, S. v. Konnov, F. Dubray, N. Nesterenko, J. P. Gilson and S. Mintova, *Angew. Chem.*, 2020, 2–21.
- 144 G. Zichittella, P. Hemberger, F. Holzmeier, A. Bodi and J. Pérez-Ramírez, *J. Phys. Chem. Lett.*, 2020, **11**, 856–863.
- 145 X. Zhang, R. You, Z. Wei, X. Jiang, J. Yang, Y. Pan, P. Wu, Q. Jia, Z. Bao, L. Bai, M. Jin, B. Sumpter, V. Fung, W. Huang and Z. Wu, *Angew. Chem., Int. Ed.*, 2020, 59, 8042–8046, DOI: 10.1002/anie.202002440.
- 146 D. Fu, O. van der Heijden, K. Stanciakova, J. E. Schmidt and B. M. Weckhuysen, *Angew. Chem., Int. Ed.*, 2020, **59**, 15502–15506, DOI: 10.1002/anie.201916596.